University of Twente

Faculty of Electrical Engineering,
Mathematics & Computer Science

Analysis and comparison of switch-based frequency converters

Michiel Soer
MSc. Thesis
September 2007

Supervisors:
prof. dr. ir. B. Nauta
dr. ing. E.A.M. Klumperink
Z. Ru MSc
dr. ir. P.T. de Boer

Report number: 067.3226
Chair of Integrated Circuit Design
Faculty of Electrical Engineering,
Mathematics & Computer Science
University of Twente
P. O. Box 217
7500 AE Enschede
The Netherlands

Abstract

Among radio amateurs a variation of the sampling mixer with 25% duty cycle is used, which is known under several names: Tayloe Product Detector, van Graas Detector or Quadrature Sampling Detector. Although the circuit has been in use for several years no thorough analysis of its properties has been made and it has not been noticed in professional scientific literature. The experimental data suggests that the circuit has low conversion loss and noise figure, while having a high linearity.

The goal of this Master Thesis is to investigate the precise properties of this mixer and to compare its performance with better known mixer circuits. The outcome is to be verified using circuit simulations. Also the feasibility of designing a RF receiver front end in 65 nm CMOS using this mixer should be explored.

A comparison has been made between the topologies of the switching, sampling and Tayloe mixer. A model topology has been found that describes all three mixers, called the frequency converter model. This model has been analyzed using Linear Periodically Time-Variant theory and closed form expressions for the periodic transfer function have been derived. From these expressions, properties like conversion gain, noise figure and baseband bandwidth can be derived.

Also an approximation of the periodic transfer function has been formulated for narrowband channels, which directly translates the duty cycle parameter to conversion gain and Noise Figure, and the bandwidth parameter to the baseband bandwidth. It was concluded that a double balanced Tayloe mixer with 25% duty cycle provides the best balance between noise figure and conversion loss.

Using these results a RF receiver front end was designed and simulated in 65 nm CMOS. The channel was chosen at 1 GHz with 20 MHz bandwidth. A conversion gain of 10.5 dB was achieved with a noise figure of 5.0 dB. Furthermore, the IIP3 is +12 dBm and the -1dB compression point is -5 dBm. Therefore, it can be concluded that a receiver front end with high linearity and moderate noise figure can be implemented using the Tayloe mixer.

Contents

List of symbols

A_k,B_k,C_k	state matrices of the k-th periodic phase
A_c	voltage conversion gain
D	number of periodic phases in a periodic system
F	noise factor
f_i	input frequency
f_o	output frequency
f_{rc}	cuttoff frequency of RC filter
f_s	clock frequency
G_x	discrete expression for the state values on switch instances
H_n	periodic transfer function
I	identity matrix
IIP3	input-referred Intercept point for 3rd order intermodulation distortion
k	index of periodic phase
n	harmonic index: $f_o = f_i + nf_s$
NF	noise figure in dB
p_k	duty cycle of k-th periodic phase
SNR	signal power to noise power ratio
t_k	start time of k-th periodic phase
T_s	clock time period $T_s = \frac{1}{f_s}$
U	input signal in the Fourier frequency domain
X	system states in the Fourier frequency domain
Y	output signal in the Fourier frequency domain

Chapter 1

Introduction

A few years ago Dan Tayloe has patented a seemingly new type of mixer circuit called the Tayloe Product Detector [1]. It is also known as the Quadrature Sampling Detector and is in use in several amateur radio receivers. A similar concept has been described by van Graas almost a decade earlier [2] and by Japanese radio amateurs [3]. In lack of a better name the circuit will be called the Tayloe Mixer in this report.

The circuit topology is much alike a sampling mixer, but is reported to have a much lower noise figure while having low conversion gain. Because it is a passive mixer, the linearity is expected to be high. In professional literature no references to this design have been found, Leung for example only describes the switching and sampling mixer [7]. Pekau and Haslett seem to have the same circuit topology but report a noise figure that is 20 dB higher [4]. Jakonis and Svensson also describe a sampling mixer with a noise figure 20 dB higher then the Tayloe Mixer is claimed to have [5].

So the question arises in what respect the Tayloe Mixer is different from the switching and sampling mixer, and what its exact properties are. Tayloe gives an approximate calculation of the conversion gain of the Tayloe Mixer [1], but provides no solid mathematical model in the time domain nor in the frequency domain. Therefore, the goal of this Master Thesis is to investigate the precise properties of this mixer and to compare its performance with better known mixer circuits. Also the feasibility of designing a RF receiver front end in 65 nm CMOS using this mixer are explored.

Chapter 2 first gives an overview and simple time domain example of the three mixer types, single balanced circuits as well as double balanced circuits. Then in chapter 3 the mathematical tools for analyzing mixers called Linear Periodically Time Variant theory is described. Using this theory the mixer types are analyzed in chapter 4, resulting in periodic transfer functions. Then in chapter 5 these transfer functions are examined further and the relationship between the three mixer types is explored. In chapter 6 the design and simulation of a RF receiver front end using the Tayloe mixer are discussed. Finally, chapter 7 provides the conclusions and chapter 8 gives some recommendations for further research.

Chapter 2

Mixer Overview

This chapter gives an overview of the two main passive mixer types used in current designs, as well as the new Tayloe mixer. The functioning of each mixer type is illustrated with a simple example in the time-domain.

2.1 Switching Mixer

The switching mixer is the simplest implementation for a mixer. The input signal is multiplied by a 50% duty cycle block wave, thus performing the mixing operation.

2.1.1 Single balanced

The single balanced switching mixer multiplies the input signal with a binary 50 percent block wave having frequency f_s to obtain frequency translation, see figure 2.1. Two switches alternately connect the RC load to the signal and to ground. It is assumed in this simple overview that the cutoff frequency of the RC filter is very high.

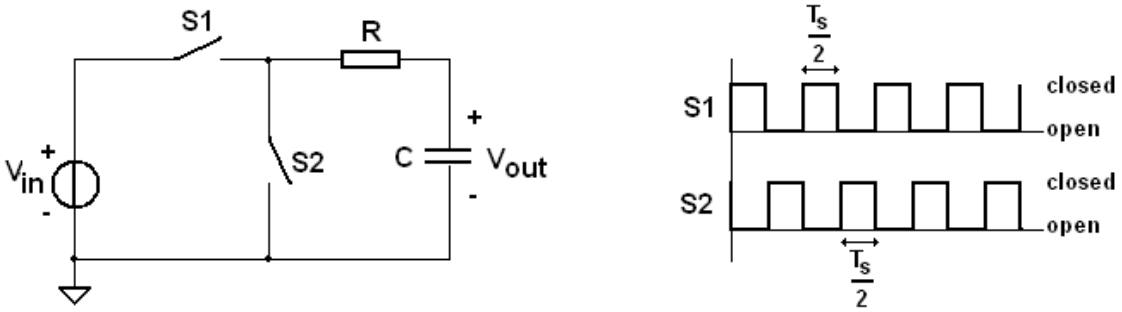

Figure 2.1: Single balanced switching mixer

When a sinusoid with a frequency equal to the clock frequency f_s is applied to the input and the switching is in phase so that the maximum conversion gain is achieved, the waveforms are approximated by (figure 2.2):

$$V_{in}(t) = sin(2\pi f_s t) \tag{2.1}$$

$$V_{out}(t) = \begin{cases} sin(2\pi f_s t) & 0 < t < \frac{T_s}{2} \\ 0 & \frac{T_s}{2} < t < T_s \end{cases} \tag{2.2}$$

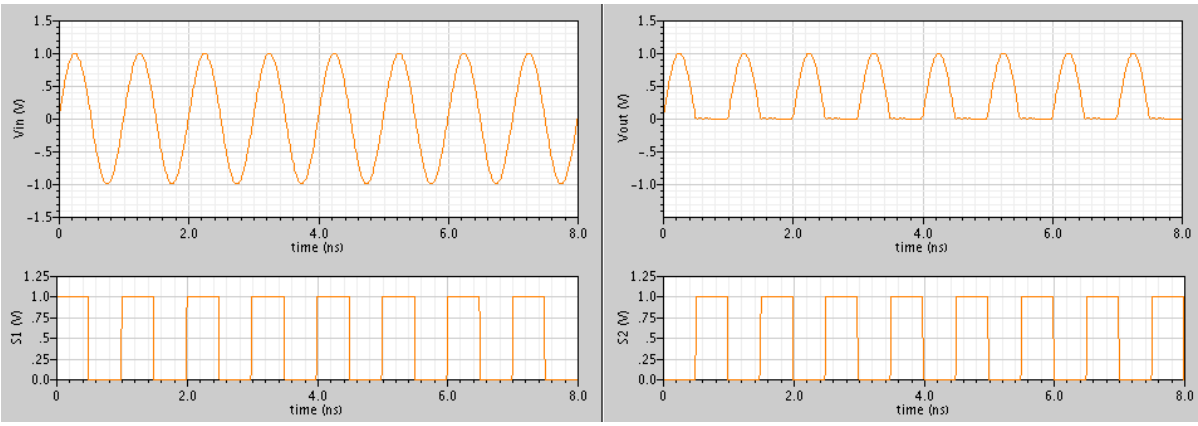

Figure 2.2: Single balanced sample waveform

Conversion gain is calculated roughly by assuming that half of the waveform is clipped away:

$$A_c = \frac{1}{T_s}\int_0^{\frac{T_s}{2}} sin(\frac{2\pi}{T_s}t)dt = \frac{1}{\pi} \cong -9.9dB \tag{2.3}$$

The noise figure is 6.9 dB, of which 3 dB is contributed by the noise in the image band (single sideband noise).

2.1.2 Double balanced

Double balancing the switching mixer results in the circuit shown in figure 2.3. Because the input signal is double balanced now it can be easily multiplied by -1 through switching the input wires. So during half the time the switching mixer follows the input signal and during the other half it follows the negated input signal.

When a sinusoid with a frequency equal to the clock frequency f_s is applied to the input and the switching is in phase so that the maximum conversion gain is achieved, the waveforms are approximated by (figure 2.4):

$$V_{in}(t) = sin(2\pi f_s t) \tag{2.4}$$

$$V_{out}(t) = \begin{cases} sin(2\pi f_s t) & 0 < t < \frac{T_s}{2} \\ -sin(2\pi f_s t) & \frac{T_s}{2} < t < T_s \end{cases} \tag{2.5}$$

Conversion gain is calculated roughly as:

$$A_c = \frac{1}{T_s}(\int_0^{\frac{T_s}{2}} sin(\frac{2\pi}{T_s}t)dt + \int_{\frac{T_s}{2}}^{T_s} -sin(\frac{2\pi}{T_s}t)dt) = \frac{2}{\pi} \cong -3.9dB \tag{2.6}$$

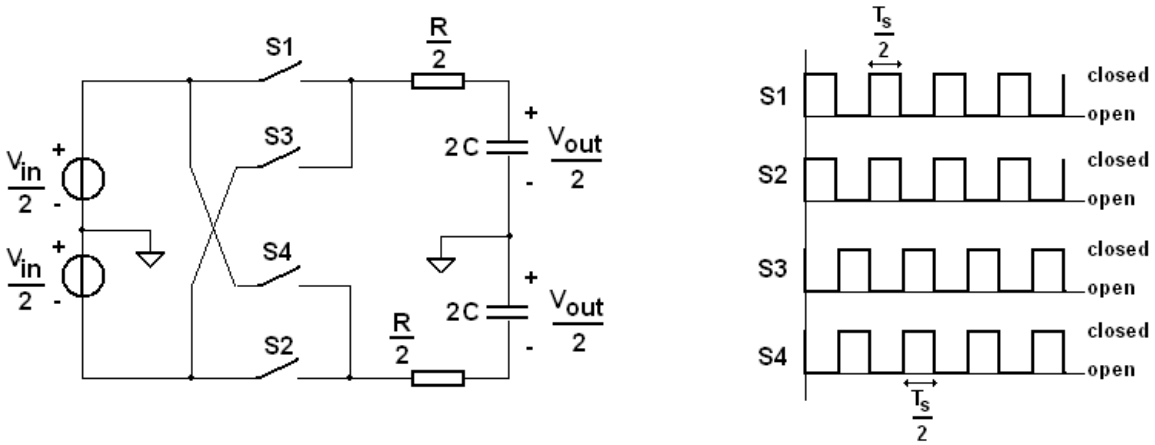

Figure 2.3: Double balanced switching mixer

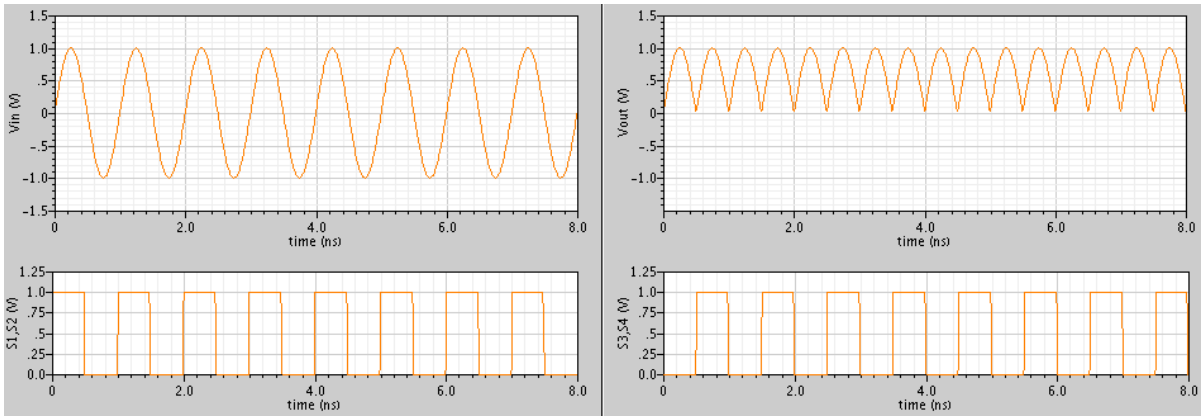

Figure 2.4: Double balanced sample waveform

Which is an improvement of 6 dB. The noise figure is also improved to 3.9dB, which is close to the limit of 3 dB.

2.2 Sampling Mixer

In a sampling mixer, a capacitor tracks and holds the input signal. The duty cycle can be very low, resulting in a low conversion loss.

2.2.1 Single balanced

The single balanced sampling mixer is shown in figure 2.5. When the switch is closed, the capacitor tracks the input signal. When the switch opens, the instantaneous input voltage is hold on the capacitor not unlike a sample and hold. In this example a duty cycle of 10 percent is used.

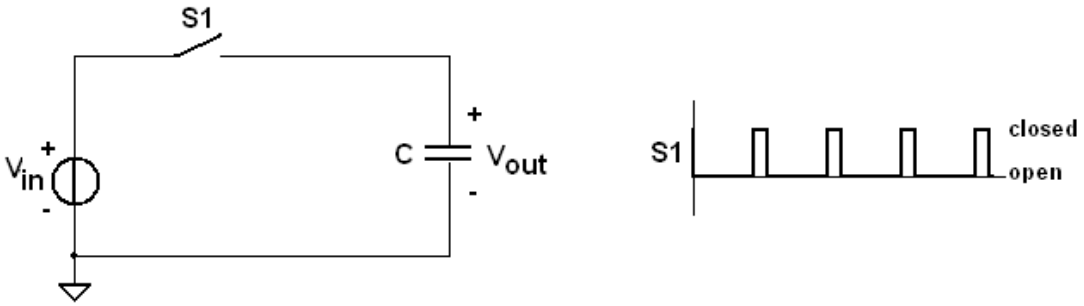

Figure 2.5: Single balanced sampling mixer

When a sinusoid with a frequency equal to the clock frequency f_s is applied to the input and the switching is in phase so that the maximum conversion gain is achieved, the waveforms are approximated by (figure 2.6):

$$V_{in}(t) = cos(2\pi f_s t) \tag{2.7}$$

$$V_{out}(t) = \begin{cases} cos(2\pi f_s t) & 0 < t < \frac{T_s}{10} \\ cos(2\pi \frac{1}{10}) & \frac{T_s}{10} < t < T_s \end{cases} \tag{2.8}$$

Conversion gain is calculated roughly as the average of the voltage on the capacitor:

$$A_c = \frac{1}{T_s}\left(\int_0^{\frac{T_s}{10}} cos(\frac{2\pi}{T_s}t)dt + \frac{9T_s}{10} cos(\frac{2\pi}{T_s}\frac{T_s}{10})\right) \cong -1.7dB \tag{2.9}$$

Which is higher then the switching mixer by several dB. By raising the duty cycle further, lower conversion losses can be achieved. When the duty cycle is almost 0 % the circuit becomes a pure sampler with zero-order-hold. The noise figure of the sampling mixer is infinite because of the sampling nature of the capacitor hold. When the switch opens a sample is taken from the instantaneous input voltage, which in the frequency domain can be interpreted as aliasing.

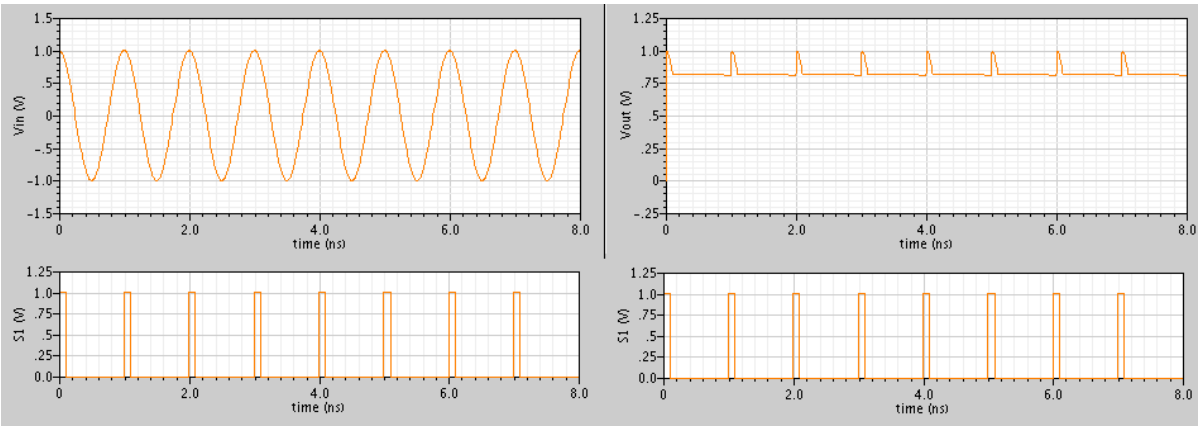

Figure 2.6: Single balanced sample waveform

2.2.2 Double balanced

The double balanced sampling mixer is very similar to the single balanced one, see figure 2.7. The input is tracked twice (during the second track the input is negated) and the hold time is halved.

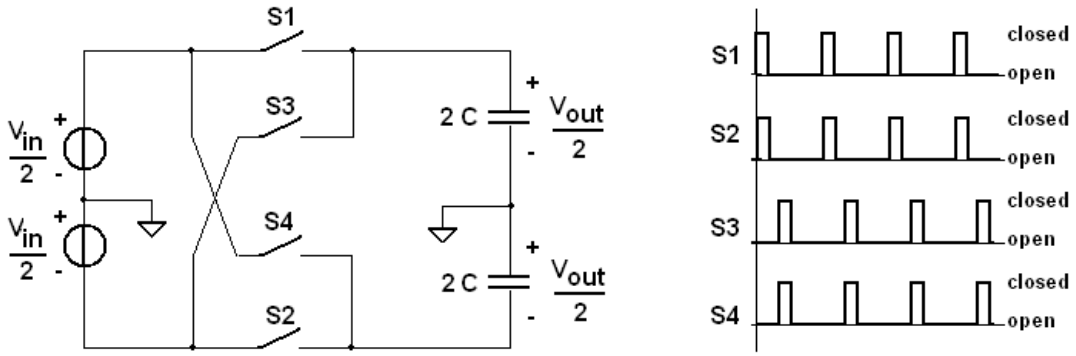

Figure 2.7: Double balanced sampling mixer

When a sinusoid with a frequency equal to the clock frequency f_s is applied to the input and the switching is in phase so that the maximum conversion gain is achieved, the waveforms are approximated by (figure 2.8):

$$V_{in}(t) = cos(2\pi f_s t) \tag{2.10}$$

$$V_{out}(t) = \begin{cases} cos(2\pi f_s t) & 0 < t < \frac{T_s}{10} \\ cos(2\pi \frac{T_s}{10}) & \frac{T_s}{10} < t < \frac{T_s}{2} \\ -cos(2\pi f_s t) & \frac{T_s}{2} < t < \frac{6T_s}{10} \\ -cos(2\pi \frac{6}{10}) & \frac{6T_s}{10} < t < T_s \end{cases} \tag{2.11}$$

Conversion gain is calculated roughly as:

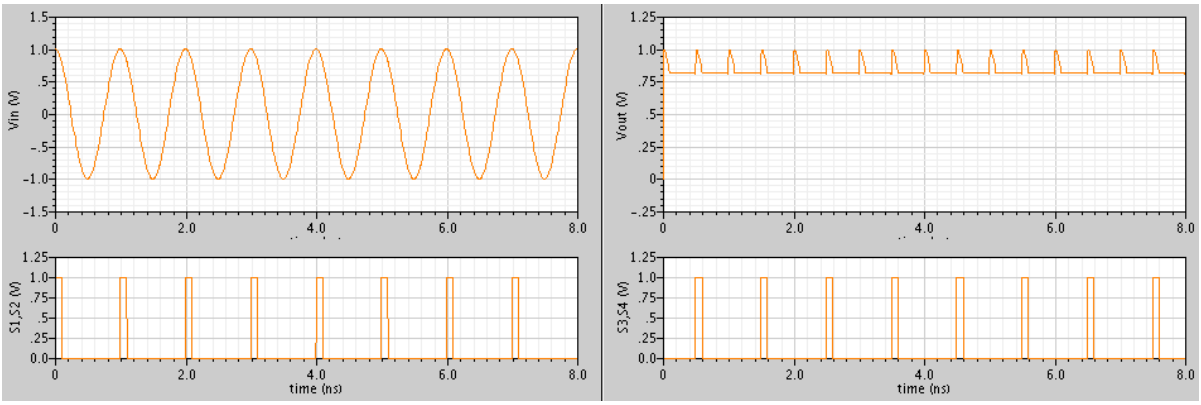

Figure 2.8: Double balanced sample waveform

$$A_c = \frac{1}{T_s}\left(\int_0^{\frac{T_s}{10}} cos(\frac{2\pi}{T_s}t)dt + \frac{4T_s}{10}cos(\frac{2\pi}{T_s}\frac{T_s}{10})\right. \tag{2.12}$$

$$\left. + \int_{\frac{5T_s}{10}}^{\frac{6T_s}{10}} -cos(\frac{2\pi}{T_s}t)dt - \frac{4T_s}{10}\cdot cos(\frac{2\pi}{T_s}\frac{6T_s}{10})\right) \cong -1.6dB \tag{2.13}$$

Which is almost the same as the single balanced sampling mixer. Again, the noise figure is infinite due to the sampling nature. So double balancing the sampling mixer has almost no effect on performance. Setting the duty cycle to almost 0%, a pure double balanced sampler with zero-order-hold is aquired with 0 dB conversion loss and infinite noise figure.

2.3 Tayloe Mixer

A special form of the sampling mixer with 25% duty cycle was patented by Dan Tayloe [1]. This mixer type is not referenced in professional literature but is known among radio amateurs.

2.3.1 Single balanced

The Tayloe mixer is actually an extension of the idea of a sampling mixer. In a sampling mixer the input signal is tracked and hold on a capacitor. This idea is extended by adding an extra resistor to limit the bandwidth of the mixer, see figure 2.9. The RC filter now averages the input signal when the switch is on.

In this example, a sinusoid with a frequency equal to the clock frequency f_s is applied to the input and the switching is in phase as to achieve maximum conversion gain. In the time domain, the mixer is seen to average the samples taken when the switch is closed (figure 2.10).

Conversion gain is calculated roughly as:

$$A_c = \frac{4}{T_s}\int_{-\frac{T_s}{8}}^{\frac{T_s}{8}} cos(\frac{2\pi}{T_s}t)dt \cong -0.9dB \tag{2.14}$$

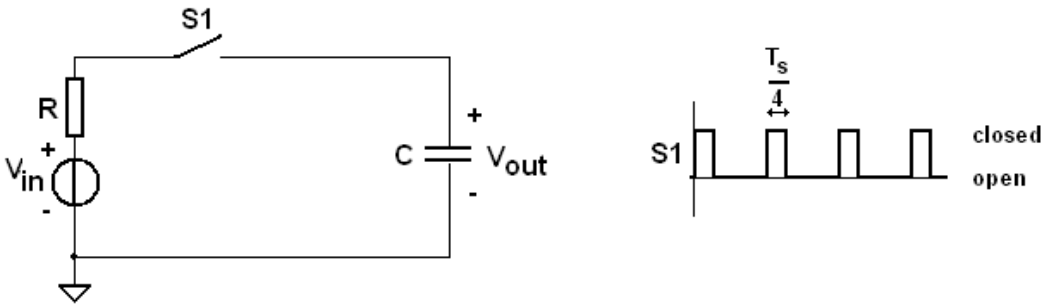

Figure 2.9: Single balanced tayloe mixer

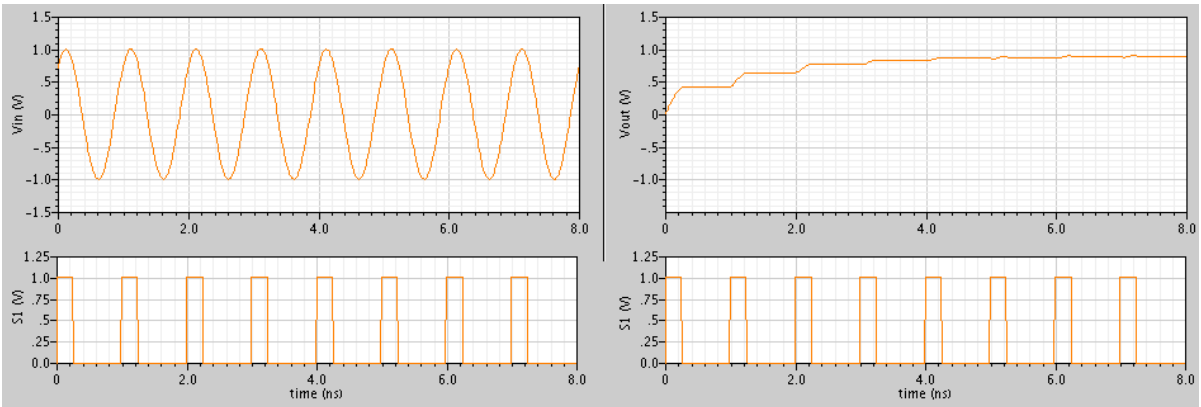

Figure 2.10: Single balanced sample waveform

In the time-domain, it is hard to generate a closed form expression for the response of the Tayloe mixer. When the switch closes the response is depended of the voltage on the capacitor, put there the previous time the switch was closed. Therefore, previous voltages on the capacitor influence the response of the circuit, resulting in a memory-like effect. No efforts have been made to solve this behavior in the time-domain. In the frequency-domain there is a closed form expression possible, as is proved in the next chapter.

2.3.2 Double balanced

As with the sampling mixer, the double balanced Tayloe mixer is very similar to the single balanced one. Figure 2.11 shows the double balanced circuit.

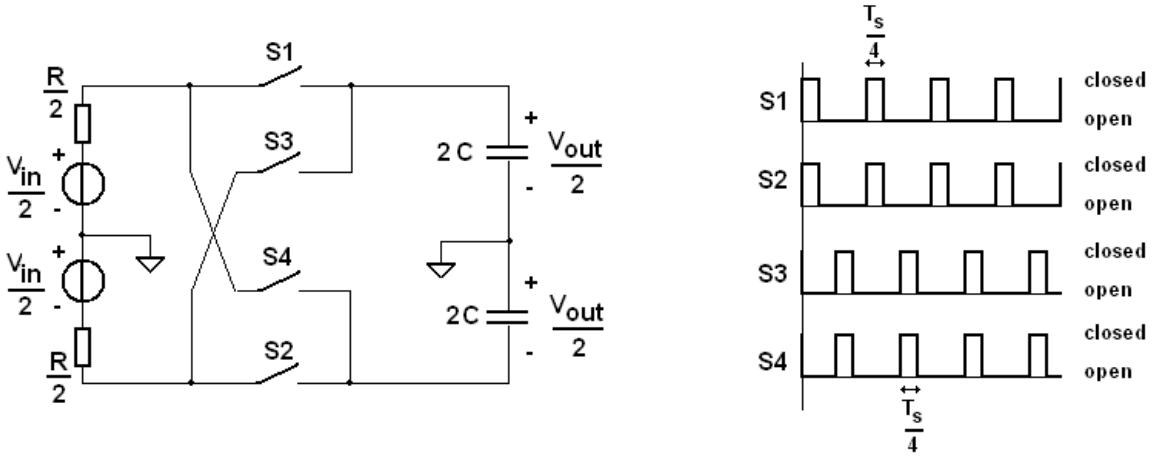

Figure 2.11: Double balanced tayloe mixer

In this example, a sinusoid with a frequency equal to the clock frequency f_s is applied to the input and the switching is in phase as to achieve maximum conversion gain (figure 2.12).

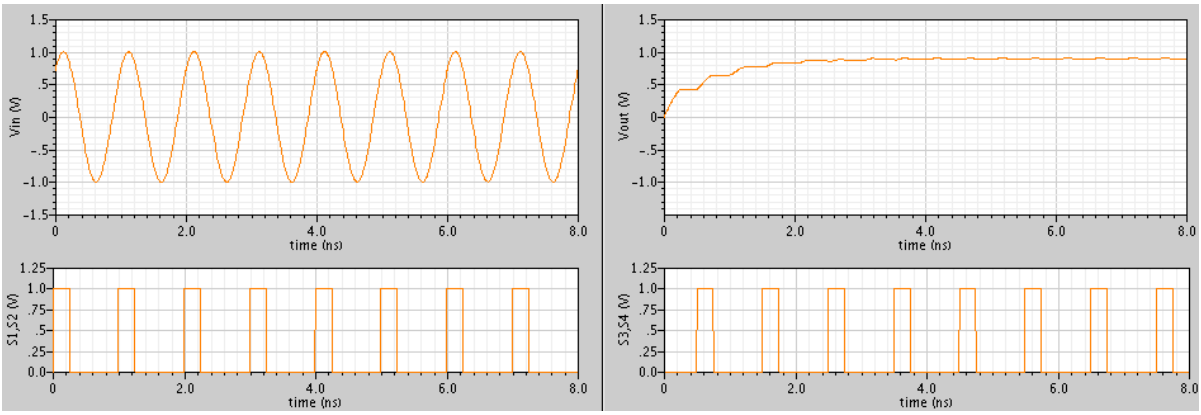

Figure 2.12: Double balanced sample waveform

Conversion gain is calculated roughly as:

$$A_c = \frac{4}{T_s}\int_{-\frac{T_s}{8}}^{\frac{T_s}{8}} cos(\frac{2\pi}{T_s}t)dt \cong -0.9dB \tag{2.15}$$

Again, a time-domain description of the double balanced mixer is difficult to generate. Therefore it will be analyzed in the frequency domain.

2.4 Frequency Converter Model

The three mixers discussed so far can be derived from a more general circuit topology, named the frequency converter model. The properties of this model are determined by two parameters: the duty cycle and the bandwidth.

2.4.1 Single Balanced

The circuits of the single balanced sampling mixer in figure 2.5 and the single balanced Tayloe mixer in figure 2.9 are very similar in circuit topology but differ in the circuit parameters. The frequency converter model in figure 2.13 can be transformed into these two mixers by setting the duty cycle p_0 and the bandwidth $f_{rc} = \frac{1}{2\pi RC}$.

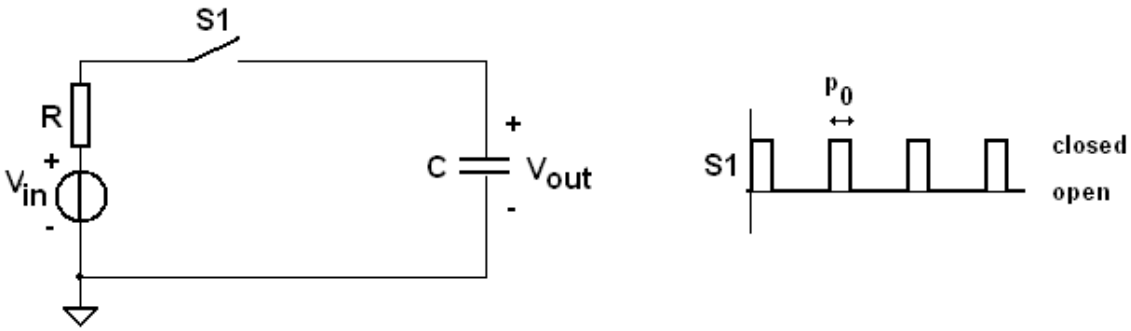

Figure 2.13: Single balanced frequency converter model

When a frequency domain description is found for this model, the expressions for the single balanced sampling and Tayloe mixer can be derived by setting the right parameters.

2.4.2 Double Balanced

The circuits of the double balanced switching mixer in figure 2.3, the double balanced sampling mixer in figure 2.7 and the double balanced Tayloe mixer in figure 2.11 are very similar in circuit topology but differ in the circuit parameters. The frequency converter model in Figure 2.14 can be transformed into these three mixers by setting the duty cycle p_0 and the bandwidth $f_{rc} = \frac{1}{2\pi RC}$.

When a frequency domain description is found for this model, the expressions for the double balanced switching, sampling and Tayloe mixer can be derived by setting the right parameters.

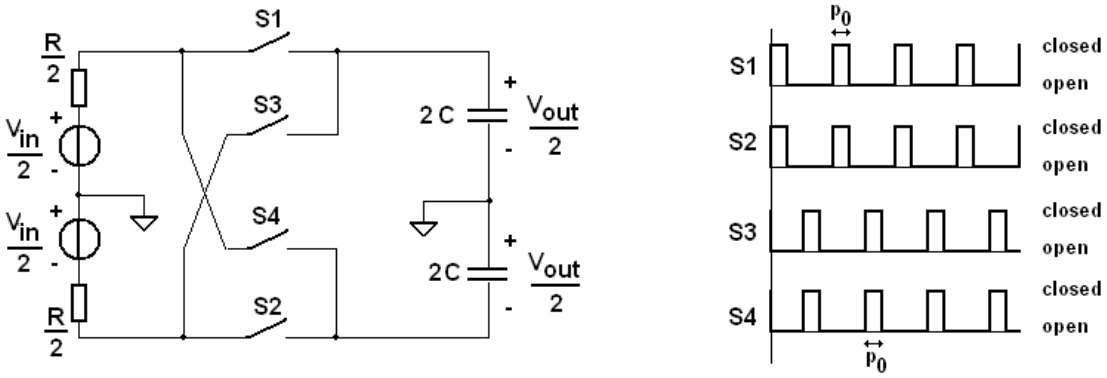

Figure 2.14: Double balanced frequency converter model

2.5 Summary

The switching mixer is always designed with 50 % duty cycle , resulting in a conversion loss of $3.9dB$ and Noise Figure of $3.9dB$. The sampling mixer has a freely defined duty cycle and can achieve much lower conversion losses, up to the point where it becomes a real sampler and the conversion loss is $0dB$. However, its sampler like nature introduces an infinite Noise Figure. The Tayloe Mixer is alike a sampling mixer with 25% duty cycle, but suppresses the noise folding by introducing an RC filter with cutoff frequency lower then the sampling frequency, resulting in a conversion loss of $0.9dB$ and a finite Noise Figure of $3.9dB$.

All mixers discussed except the single balanced switching mixer are generalizations of the frequency converter model defined in section 2.4. Any analysis done for the frequency converter model can be converted to the mixer types by setting the duty cycle and bandwidth parameters. The time domain simulation is not suitable for providing specific information about conversion loss and Noise Figure, so a frequency domain approach is needed to determine which mixer gives the best performance.

Chapter 3

Linear Periodically Time Variant Systems

For the frequency-domain analysis of frequency translating circuits (like mixers) it is insufficient to use Linear Time Invariant system theory. The LTI system theory has been extended for periodically time-variant systems, which are systems with a finite number of periodically cycling linear time-invariant responses. This chapter describes Linear Periodically Time Variant (LPTV) theory and a method for calculating the LPTV response for switching circuits.

3.1 The periodic transfer function

The most commonly used type of circuit in Electrical Engineering is the Linear Time Invariant or LTI system. The theory behind such circuits is well understood en can be intuitively used to analyze and design LTI circuits. A different set of circuits can be described as a Linear Periodically Time Variant or LPTV circuit. Again the circuit is linear, but its response changes periodically in time. This means that its impulse response is repetitive with a certain period T_s. Examples of LPTV circuits are usually build out of LTI elements and periodically operated switches.

Leung gives a quick introduction in the basics of LPTV systems [7]. In a LPTV system the impulse response is dependent on the time the impulse stimulus is presented to the circuit. Called the periodic impulse response, it is denoted with $g(v,u)$ and is dependent on the two time variables v and u. v is the time the impulse stimulus is presented to the input of the system (also called the launch time) and u is the time elapsed after the impulse stimulus. In a LPTV system, $g(v,u)$ is periodic in v with period T_s. Therefore, the periodic impulse response can be represented as a Fourier series with periodic frequency $f_s = \frac{1}{T_s}$:

$$g_n(v) = \frac{1}{T_s}\int_0^{T_s} g(v,u)e^{-j2\pi n f_s u}du \tag{3.1}$$

From the convolution of input and impulse response, we can derive the frequency reponse of the LPTV system as :

$$Y(f_o) = \sum_{n=-\infty}^{\infty} H_n(f_o)U(f_o - nf_s) \tag{3.2}$$

$$H_n(f_o) = \int_{-\infty}^{\infty} g_n(v)e^{j2\pi f_o v}dv \tag{3.3}$$

This periodic transfer function can also be written in term of the input frequency $f_i = f_o - nf_s$, resulting in the reciprocal:

$$Y(f_o) = \sum_{n=-\infty}^{\infty} H_n(f_i + nf_s)U(f_i) \tag{3.4}$$

The output spectra of the LPTV system is constructed from an infinite number of shifted input spectra multiplied by their specific transfer function. The transfer function is now two-dimensional in n: the harmonic index and f_o: the output frequency. By controlling the transfer function in the n dimensionality, it is possible to control the amount of spectrum that is folded back. This folding property proves useful for mixer circuits, which are supposed to do a frequency translation. In most practical systems, it is necessary to limit the transfer function in the n dimension, as to limit the number of spectra folded back into the output. Therefore H_n should be designed to asymptotically go to zero for larger n.

3.2 Strom and Signell theory

For some specific problems the periodic transfer function can be found using Fourier frequency analysis and transforming the result to the form of equation 3.3. The switching and sampling mixer can be analyzed using this method, but the Tayloe Mixer and frequency converter model cannot. A more general methodology for solving LPTV systems is given in the work of Strom and Signell [6]. Their method is used to obtain a closed form expression for the frequency converter model.

In the time intervals between switching moments, an LPTV system has a defined LTI response, which is only valid in the switching interval. The switching interval is referred to as one of the periodic phases of the LPTV system. Strom and Signell describe a method for expanding the LTI description until it is valid for the complete time. Then each periodic phase can be processed with LTI techniques and the summation of all states forms the overall response.

The periodic phase $nT_s < t < nT_s + T_s$ can be divided into D portions (or states), each portion having an LTI response. The k-th state is then referred to as the time period $nT_s + t_k < t < nT_s + t_{k+1}$ for $k = 0, .., D-1$. The duty cycle of each state interval is then defined as $p_k = \frac{t_{k+1} - t_k}{T_s}$ for $k = 0, .., D-1$. Each k-th state then has a valid LTI state space description within the interval:

$$\begin{aligned} \frac{d}{dt}x_k(t) &= A_k x_k(t) + B_k u(t) \\ y(t) &= C_k x_k(t) \end{aligned} \tag{3.5}$$

This LTI description is only valid within $nT_s + t_k < t < nT_s + t_{k+1}$, so to be able to use Fourier analysis the differential equation has to be made valid in the interval $-\infty < t < \infty$. In order to keep the states separated, the output of each state must only be non-zero inside its interval. Therefore the functions $y_k(t)$ and $u_k(t)$ are defined, which are equal to $y(t)$ and $u(t)$ inside the k-th interval, and equal to zero outside the k-th interval:

$$y_k(t) = y(t)\delta_{k(t),k} \tag{3.6}$$

$$u_k(t) = u(t)\delta_{k(t),k} \tag{3.7}$$

where $\delta_{k(t),k}$ is the indicator function which is 1 inside the k-th interval and 0 outside the k-th interval. The indicator function for a state is shown in figure 3.1. The indicator function can be expressed in a Fourier series and has the discrete spectrum:

$$\delta_{k(t),k}(f) = \sum_{n=-\infty}^{\infty} \frac{e^{-j2\pi n f_s t_k} - e^{-j2\pi n f_s t_{k+1}}}{j2\pi n} \delta(f - nf_s) \tag{3.8}$$

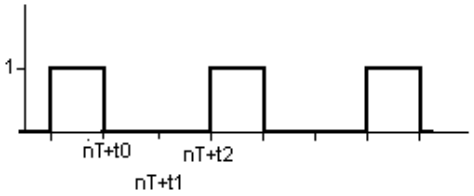

Figure 3.1: Indicator function for $D = 3$ and $k = 2$

In order to comply to equation 3.7, the LTI differential equation for the k-th state has to be modified to:

$$\begin{aligned} \frac{d}{dt}x_k(t) &= A_k x_k(t) + B_k u_k(t) + \\ &\sum_{n=-\infty}^{\infty} x_k(t)\delta(t - nT_s - t_k) - x_k(t)\delta(t - nT_s - t_{k+1}) \\ &= A_k x_k(t) + B_k u_k(t) + \\ &\sum_{n=-\infty}^{\infty} x_k(nT_s + t_k)\delta(t - nT_s - t_k) - x_k(nT_s + t_{k+1})\delta(t - nT_s - t_{k+1}) \end{aligned} \tag{3.9}$$

$$y_k(t) = C_k x_k(t) \tag{3.10}$$

Inspection reveals that at the beginning of the state interval the initial value of the state is injected using a delta pulse, while at the end of the state interval the final value of the state is subtracted using a delta pulse. Together with the replacement of $u(t)$ with $u_k(t)$ this ensures that $x_k(t)$ is zero outside $nT_s + t_{k-1} < t < nT_s + t_k$ and equal to $x(t)$ inside the interval. The total response of the system is now the sum of the D states:

$$y(t) = \sum_{k=0}^{D-1} y_k(t) \tag{3.11}$$

The discrete values of x_k (initial and final values of the interval) can be solved using the D-dimensional difference equation with a sinusoid as input:

$$x_k(nT_s + t_{m+1}) - L_m x_k(nTs + t_m) = M_m e^{-j2\pi f n T_s}, m = 0, .., D - 1 \tag{3.12}$$

where the expressions L_m and M_m are determined by the Laplace equation of the m-th LTI response. The solution can be calculated using the Z-transform and has the form:

$$x_k(nTs + t_m) = G_m(f_i) e^{-j2\pi f_i n T_s}, m = 0, .., D - 1 \tag{3.13}$$

Note that this solution for x_k is only valid on the switching instances and $G_m(f_i)$ is cyclic: $G_0(f_i) = G_{D-1} e^{j2\pi f_i T_s}$.

By inserting equation 3.13 into equation 3.10 and taking the Fourier transform of the result, the following expression is obtained:

$$\begin{aligned} X_k(f_o)(j2\pi f_o I - A_k) = \sum_{n=-\infty}^{\infty} [B_k(U(f_o)) * (\delta(f_o - nf_s)\frac{e^{-j2\pi n f_s t_{k-1}} - e^{-j2\pi n f_s t_k}}{j2\pi n}) \\ + (G_{k-1}(f_o)U(f_o)) * \delta(f_o - nf_s) \cdot f_s e^{-j2\pi f_o t_k} \\ - (G_k(f_o)U(f_o)) * \delta(f_o - nf_s) \cdot f_s e^{-j2\pi f_o t_{k+1}}] \end{aligned} \tag{3.14}$$

$$Y(f_o) = \sum_{k=1}^{D} C_k X_k(f_o) \tag{3.15}$$

By evaluating the delta functions, this reduces to:

$$\begin{aligned} X_k(f_o) = \sum_{n=-\infty}^{\infty} (j2\pi f_o I - A_k)^{-1}[B_k \frac{e^{-j2\pi n f_s t_{k-1}} - e^{-j2\pi n f_s t_k}}{j2\pi n} \\ + f_s G_{k-1}(f_o - nf_s) e^{-j2\pi(f_o - nf_s)t_k} e^{-j2\pi n f_s t_k} \\ - f_s G_k(f_o - nf_s) e^{-j2\pi(f_o - nf_s)t_{k+1}} e^{-j2\pi n f_s t_{k+1}}] U(f_o - nf_s) \end{aligned} \tag{3.16}$$

And by making notice that $e^{-j2\pi n f_s t_{k+1}} = e^{-j2\pi n f_s t_k} e^{-j2\pi n p_k}$ a common phase factor is split off:

$$\begin{aligned} X_k(f_o) = \sum_{n=-\infty}^{\infty} e^{-j2\pi n f_s t_k} (j2\pi f I - A_k)^{-1} \big[B_k \frac{1 - e^{-j2\pi n p_k}}{j2\pi n} \\ + f_s G_k(f_i) e^{-j2\pi f_i t_k} - f_s G_{k+1}(f_i) e^{-j2\pi f_i t_{k+1}} e^{-j2\pi n p_k}\big] U(f_o - nf_s) \end{aligned} \tag{3.17}$$

The calculation of the frequency response of a LPTV system involves the following steps:

- Define D states with proper LTI differential equations
- Find the Laplace transform of each LTI differential equation
- Solve the D dimensional difference equation to obtain the initial and final values for each state
- Solve the LTI frequency response for each LTI differential equation
- Evaluate and simplify equation 3.17 for each state
- Sum the responses from all states into:

$$\begin{aligned} Y(f_o) &= \sum_{k=0}^{D-1} C_k X_k(f_o) \\ &= \sum_{k=0}^{D-1} \sum_{n=-\infty}^{\infty} C_k H_{n,k}(f_o) U(f_o - nf_s) \end{aligned} \tag{3.18}$$

Figure 3.2: LPTV analysis

3.3 Properties of the periodic transfer function

3.3.1 Symmetry

A fundamental property of the periodic transfer function defined in equation 3.3 is the symmetry in the $f = nf_s$ line:

$$H_n(f) = H^*_{-n}(-f) \tag{3.19}$$

a property proved in [6]. This is closely related to the symmetry property of an LTI system which ensure that the complex spectra represent real signals:

$$H(f) = H^*(-f) \tag{3.20}$$

3.3.2 Conversion Gain and Noise Figure

When a mixer is build from a LPTV system, the goal is to translate a single piece of spectrum once through the frequency spectrum without additional components. Since the frequency response of the LPTV system is given by:

$$Y(f_o) = \sum_{n=-\infty}^{\infty} H_n(f_o)U(f_o - nf_s) \tag{3.21}$$

$$Y(f_o) = \sum_{n=-\infty}^{\infty} H_n(f_i + nf_s)U(f_i) \tag{3.22}$$

the most interesting frequency translation point is with $n = \pm 1$. So, in an ideal situation the transfer function would be zero for all $n \neq -1$ and unity for $n = -1$. Because this will not be the case several figures exist to access the performance.

The gain of the input signal to the baseband is noted as the Conversion Gain and is simply $H_{-1}(f_i - f_s)$. In general, the conversion gain is frequency dependent. Because the transfer function for $n \neq -1$ is in general not equal to zero, noise in frequency bands outside the signal bandwidth are also translated to the baseband. This noise-folding deteriorates the output signal-to-noise ratio (SNR), even if the mixer components are considered noise free. The figure-of-merit for noise performance is expressed as the noise factor:

$$F = \frac{SNR_{in}}{SNR_{out}} = \frac{P_{in}}{N_{in}} \frac{N_{out}}{P_{out}} \tag{3.23}$$

Where P_{in} is the power of the input signal at the input, P_{out} is the power of the input signal at the output, N_{in} is the noise power at the input and N_{out} is the noise power at the output. For a single-sideband signal the conversion power gain is given by:

$$P_{out} = |H_{-1}(f_o)|^2 P_{in} \tag{3.24}$$

In the ideal case when the circuit components do not contribute extra noise, the only contribution to the output noise is the input noise folded by each harmonic transfer function:

$$N_{out} = \sum_{n=-\infty}^{\infty} |H_n(f_o)|^2 N_{in} = \sum_{n=-\infty}^{\infty} |H_n(f_i + nf_s)|^2 N_{in} \tag{3.25}$$

Inserting equation 3.24 and 3.25 into the noise factor equation 3.23:

$$F = \frac{P_{in}}{N_{in}} \frac{\sum_{n=-\infty}^{\infty} |H_n(f_o)|^2 N_{in}}{|H_{-1}(f_o)|^2 P_{in}} \tag{3.26}$$

$$= \frac{\sum_{n=-\infty,\text{odd}}^{\infty} |H_n(f_o)|^2}{|H_{-1}(f_o)|^2} \tag{3.27}$$

For convenience the noise factor is converted to decibels and is called the single-sided noise figure:

$$NF(dB) = 10log(F) \tag{3.28}$$

So the periodic transfer function must asymptotically go to zero as n goes to infinity to obtain a finite noise figure.

3.3.3 Time shift

The periodic transfer functions for an LPTV system is given by:

$$Y(f_o) = \sum_{n=-\infty}^{\infty} H_n(f_i)U(f_i) \tag{3.29}$$

Performing a time shift t_k on input and output:

$$Y(f_o)e^{j2\pi f_o t_k} = \sum_{n=-\infty}^{\infty} H_n(f_i)U(f_i)e^{j2\pi f_i t_k} \tag{3.30}$$

$$Y(f_o) = \sum_{n=-\infty}^{\infty} H_n(f_i)e^{j2\pi(f_i - fo)t_k}U(f_i) \tag{3.31}$$

$$= \sum_{n=-\infty}^{\infty} H_n(f_i)e^{j2\pi n f_s t_k}U(f_i) \tag{3.32}$$

So shifting the clock timing to t_k results in a factor $e^{j2\pi n f_s t_k}$ in the periodic transfer function. This factor is present in equation 3.17, but in it there is another term dependent on t_k: $G_k(f_i)e^{-j2\pi f_i t_k}$. This can only mean that $G_k(f_i)$ is of the form:

$$G_k(f_i) = G_k^{'}(f_i)e^{j2\pi f_i t_k} \tag{3.33}$$

In the $G_k(f_i)$ expressions derived in appendix B this is indeed the case.

3.3.4 Even-order Harmonic Cancellation

Equation 3.32 shows that a time shift of t_k in the clock signals results in the term $e^{-j2\pi n f_s t_k}$ in the periodic transfer function. Now imagine taking two identical LPTV systems with different phase timing, let's say that the first system starts at $t_{0,A}$ and the second system starts at $t_{0,B}$. If the zero phase delay transfer function of a system is equal to $H_{n,0}$ then their respective transfer functions are:

$$H_{n,A} = e^{-j2\pi n f_s t_{0,A}} H_{n,0} \tag{3.34}$$

$$H_{n,B} = e^{-j2\pi n f_s t_{0,B}} H_{n,0} \tag{3.35}$$

Now let $t_{0,B} = t_{0,A} + \frac{1}{2}T_s$ which resembles a timing difference of 180 degrees and subtract the outputs of the two systems, then the total transfer function becomes:

$$H_n = e^{-j2\pi n f_s t_{0,A}}(1 - e^{-j2\pi\frac{1}{2}n})H_{n,0} \tag{3.36}$$

By inspection, $(1 - e^{-j2\pi\frac{1}{2}n})$ is zero for even n and double unity for uneven n. This means that all even harmonics are cancelled. In a mixer where even harmonics are unwanted, such a mechanism is very useful. Furthermore, by combining LPTV systems in different ways more harmonic cancellation can be achieved at the cost of greater circuit complexity.

3.3.5 IQ Image Rejection

For image rejection, many receivers use a Weaver architecture as shown in figure 3.3. In this architecture, the input signal is mixed by two LO signals differing 90 degrees in phase. The mixed signals are referred to as Inphase (I) and Quadrature (Q) channels. By combining I and Q signal again the image can be completely canceled.

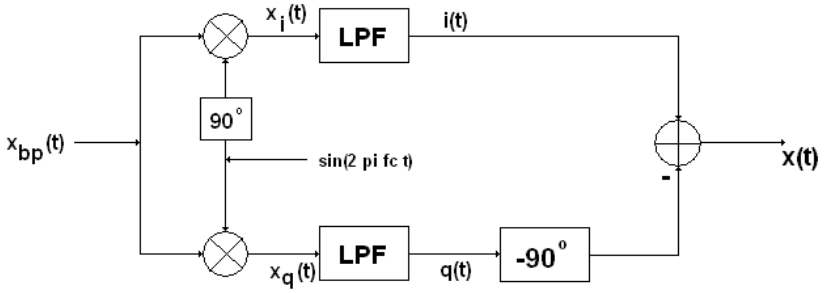

Figure 3.3: Weaver architecture

To analyze the conventional weaver architecture, let's consider a single frequency from a bandpass signal. The analysis can be made in the time or in the frequency domain, but a frequency analysis is more useful since for the LPTV systems only a transfer function is available. The bandpass sinusoid is given by:

$$x_{bp}(f) = \frac{1}{2}C(f_1)\delta(f - f_c - f_1) + \frac{1}{2}C^*(f_1)\delta(f + f_c + f_1) \tag{3.37}$$

where f_1 is the sinusoid equivalent baseband frequency and $C(f_1)$ is the equivalent baseband spectrum of the signal. Working out the multiplication with the cosine and low pass filter the result gives:

$$\begin{aligned} x_i(t) =& x_{bp}(t) * \frac{1}{2}(\delta(f - f_c) + \delta(f + fc)) && (3.38)\\ =& \frac{1}{4}C(f_1)\delta(f - f_1) + \frac{1}{4}C^*(f_1)\delta(f + 2f_c + f_1) \\ &+ \frac{1}{4}C(f_1)\delta(f - 2f_c - f_1) + \frac{1}{4}C^*(f_1)\delta(f + f_1) && (3.39)\\ i(t) =& \frac{1}{4}C(f_1)\delta(f - f_1) + \frac{1}{4}C^*(f_1)\delta(f + f_1) && (3.40) \end{aligned}$$

In similar fashion, the quadrature component is found my multiplying the signal by the sine and low pass filter the result:

$$x_i(t) = x_{bp}(t) * \frac{1}{2j}(\delta(f - f_c) - \delta(f + fc)) \tag{3.41}$$

$$= -\frac{1}{4j}C(f_1)\delta(f - f_1) - \frac{1}{4j}C^*(f_1)\delta(f + 2f_c + f_1) + \frac{1}{4j}C(f_1)\delta(f - 2f_c - f_1) + \frac{1}{4j}C^*(f_1)\delta(f + f_1) \tag{3.42}$$

$$i(t) = -\frac{1}{4j}C(f_1)\delta(f - f_1) + \frac{1}{4j}C^*(f_1)\delta(f + f_1) \tag{3.43}$$

To obtain the baseband spectrum the I and Q signal are combined:

$$x(t) = i(t) - jq(t) \tag{3.44}$$

$$= \frac{1}{2}C(f_1)\delta(f - f_1) \tag{3.45}$$

The same principles can be applied to the LPTV system, regarding the frequency response for $n = 1$ and $n = -1$ since these translate the bandpass signal to baseband. From equation 3.32 it was proved that an LPTV system can always be written in the form:

$$Y(f) = \sum_{n=-\infty}^{\infty} e^{-j2\pi n f_s t_0} H_n(f)U(f - nf_s) \tag{3.46}$$

Lets consider two identical LPTV systems with different t_0. The first, labeled I, has $t_{0,I} = 0$ while the second, labeled Q, has $t_{0,Q} = \frac{1}{4}T_s = \frac{1}{4f_s}$. The net effect is that circuit Q lags a quarter sample period behind circuit I. If the same signal is taken as in equation 3.37, the output of circuit I is calculated to be:

$$Y_I(f) = \sum_{n=-\infty}^{\infty} H_n(f)U(f - nf_s) \tag{3.47}$$

$$= \frac{1}{2}\left[C(f_1)H_1(f)\delta(f - 2f_c - f_1) + C^*(f_1)H_1(f)\delta(f + f_1)\right] + \frac{1}{2}\left[C(f_1)H_{-1}(f)\delta(f - f_1) + C^*(f_1)H_{-1}(f)\delta(f + 2f_c + f_1)\right] \tag{3.48}$$

$$I(f) = \frac{1}{2}\left[C(f_1)H_{-1}(f)\delta(f - f_1) + C^*(f_1)H_1(f)\delta(f + f_1)\right] \tag{3.49}$$

And similarly for the output of circuit Q:

$$Y_I(f) = \sum_{n=-\infty}^{\infty} e^{-j2\pi n\frac{1}{4}} H_n(f)U(f - nf_s) \tag{3.50}$$

$$= \frac{1}{2}e^{-j2\pi\frac{1}{4}}\left[C(f_1)H_1(f)\delta(f - 2f_c - f_1) + C^*(f_1)H_1(f)\delta(f + f_1)\right] + \frac{1}{2}e^{j2\pi\frac{1}{4}}\left[C(f_1)H_{-1}(f)\delta(f - f_1) + C^*(f_1)H_{-1}(f)\delta(f + 2f_c + f_1)\right] \tag{3.51}$$

$$Q(f) = \frac{1}{2}e^{-j2\pi\frac{1}{4}}C^*(f_1)H_1(f)\delta(f + f_1) + \frac{1}{2}e^{j2\pi\frac{1}{4}}C(f_1)H_{-1}(f)\delta(f - f_1) \tag{3.52}$$

Because $e^{-j2\pi\frac{1}{4}} = \frac{1}{j}$ and $e^{j2\pi\frac{1}{4}} = \frac{-1}{j}$ this equation reduces to:

$$Q(f) = \frac{1}{2j}\left[C^*(f_1)H_1(f)\delta(f + f_1) - C(f_1)H_{-1}(f)\delta(f - f_1)\right] \tag{3.53}$$

The combination of circuit I and Q then results in:

$$Y(f) = I(f) - jQ(f) \tag{3.54}$$
$$= C(f_1)H_{-1}(f)\delta(f - f_1) \tag{3.55}$$

Therefore, when an LPTV circuit is used for quadrature image rejection can be performed by having two identical LPTV circuits with a quarter sampling period lag between the state intervals.

3.4 Summary

A linear periodically time variant system folds the input spectrum multiple times with each harmonic having its own transfer function. For each harmonic n the output frequency f_o of a sinusoid with input frequency f_i is defined as $f_o = f_i + nf_s$, where f_s is the periodic switching frequency. In the frequency domain the output spectrum is obtained through:

$$Y(f_o) = \sum_{n=-\infty}^{\infty} H_n(f_o)U(f_o - nf_s) \tag{3.56}$$

With Strom and Signell theory the periodic transfer function $H_n(f_o)$ can be calculated by defining a finite number of states with valid Linear Time Invariant descriptions and summing the modified expressions according to box 3.2.

For frequency translation (mixer) the most interesting harmonic is $n = \pm 1$. Since $H_n(f_o)$ is symmetric around $n = 0$, the conversion gain can be defined either as the magnitude of $H_{n=1}$ or $H_{n=-1}$. From $H_n(f_o)$ the Noise Figure can be easily determined by evaluating:

$$NF(dB) = 10log(\frac{\sum_{n=-\infty}^{\infty} |H_n(f_o)|^2}{|H_{-1}(f_o)|^2}) \tag{3.57}$$

It was also derived that all even harmonic transfer functions (n = even) can be made zero by summing the outputs of two identical LPTV systems, with the second having a switching pattern that lags $\frac{T_s}{2}$ behind the first. Also, IQ image rejection is possible by duplicating the LPTV system again and applying a $\frac{T_s}{4}$ delay in the switching pattern.

Chapter 4

Mixer Analysis

In this Chapter the switching mixer, sampling mixer and frequency converter model are analyzed using the Linear Periodically Time Variant theory presented in the previous chapter. The derivations result in the periodic transfer function for each mixer type.

4.1 Switching Mixer

4.1.1 Single Balanced

The signal representation of the single balanced switching mixer is shown in figure 4.1.

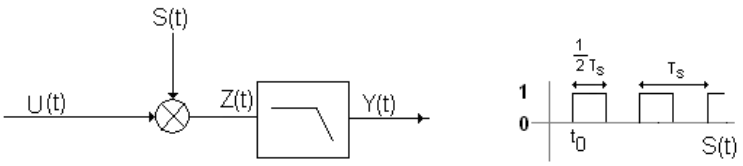

Figure 4.1: Single balanced switching mixer signal representation

The time domain description of the circuit is given by:

$$z(t) = u(t) \sum_{n=-\infty}^{\infty} \text{rect}(2\frac{t-t_0}{T_s} - 2n - \frac{1}{2}) \tag{4.1}$$

$$= u(t) \sum_{n=-\infty}^{\infty} \text{rect}(\frac{t-t_0-nT_s-\frac{1}{4}T_s}{\frac{1}{2}T_s}) \tag{4.2}$$

$$= u(t) \sum_{n=-\infty}^{\infty} \frac{1}{2}\text{sinc}(\frac{1}{2}n)e^{j2\pi n f_s(t-t_0-\frac{1}{4}T_s)} \tag{4.3}$$

paragraph After transformation to the frequency domain:

$$Z(f_o) = U(f_i) * \sum_{n=-\infty}^{\infty} \frac{1}{2}\text{sinc}(\frac{1}{2}n)\delta(f_o - nf_s)e^{-j2\pi nf_s t_0}e^{-j2\pi\frac{1}{4}n} \tag{4.4}$$

$$= \sum_{n=-\infty}^{\infty} e^{-j2\pi nf_s t_0}\frac{1}{2}\text{sinc}(\frac{1}{2}n)e^{-j2\pi\frac{1}{4}n}U(f_o - nf_s) \tag{4.5}$$

$$Y(f_o) = \sum_{n=-\infty}^{\infty} \frac{e^{-j2\pi nf_s t_0}}{1 + j\frac{f_o}{f_{rc}}}\frac{1}{2}\text{sinc}(\frac{1}{2}n)e^{-j2\pi\frac{1}{4}n}U(f_o - nf_s) \tag{4.6}$$

The resulting periodic transfer function is given in figure 4.2.

$$H_n(f_o) = \frac{e^{-j2\pi nf_s t_0}}{1 + j\frac{f_o}{f_{rc}}}\frac{1}{2}\text{sinc}(\frac{1}{2}n)e^{-j2\pi\frac{1}{4}n} \tag{4.7}$$

$$= \frac{e^{-j2\pi nf_s t_0}}{1 + j\frac{f_o}{f_{rc}}}\frac{1 - e^{-j2\pi\frac{1}{2}n}}{j2\pi n} \tag{4.8}$$

Note that $H_n(f_o)$ is decreasing with increasing n, resulting in a finite Noise Figure.

Figure 4.2: Switching Mixer Single Balanced H_n

4.1.2 Double Balanced

The signal representation of the double balanced switching mixer is shown in figure 4.3. The two branches each multiply the input signal with a 50% duty cycle blockwave and are then added together.

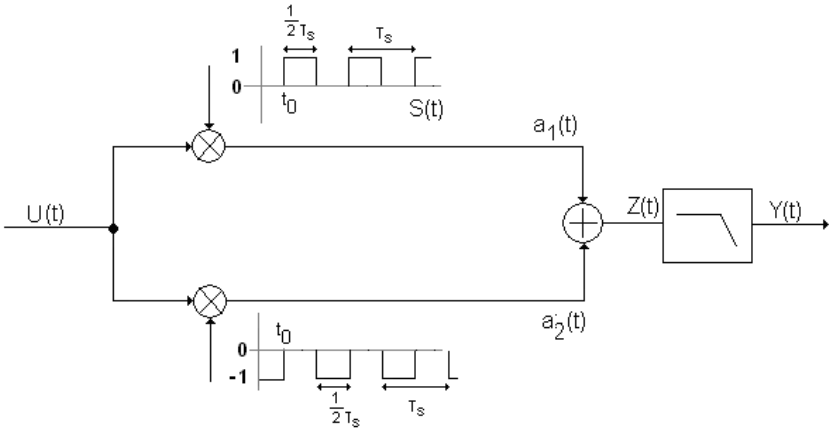

Figure 4.3: Double balanced switching mixer signal representation

The time domain description of the circuit is given by:

$$z(t) = u(t) \sum_{n=-\infty}^{\infty} \text{rect}(2\frac{t-t_0}{T_s} - 2n - \frac{1}{2}) - u(t) \sum_{n=-\infty}^{\infty} \text{rect}(2\frac{t-t_0}{T_s} - 2n - 1\frac{1}{2}) \tag{4.9}$$

$$= u(t) \sum_{n=-\infty}^{\infty} \left[\text{rect}(\frac{t-t_0-nT_s-\frac{1}{4}T_s}{\frac{1}{2}T_s}) - \text{rect}(\frac{t-t_o-nT_s-\frac{3}{4}T_s}{\frac{1}{2}T_s}) \right] \tag{4.10}$$

$$= u(t) \sum_{n=-\infty}^{\infty} \left[\frac{1}{2}\text{sinc}(\frac{1}{2}n)e^{j2\pi nf_s(t-t_0-\frac{1}{4}T_s)} - \frac{1}{2}\text{sinc}(\frac{1}{2}n)e^{j2\pi nf_s(t-t_0-\frac{3}{4}T_s)} \right] \tag{4.11}$$

After transformation to the frequency domain:

$$Z(f_o) = U(f_i) * \sum_{n=-\infty}^{\infty} \left[\frac{1}{2}\text{sinc}(\frac{1}{2}n)\delta(f_o - nf_s)e^{-j2\pi nf_s t_0}e^{-j2\pi\frac{1}{4}n} - \frac{1}{2}\text{sinc}(\frac{1}{2}n)\delta(f_o - nf_s)e^{-j2\pi nf_s t_0}e^{-j2\pi\frac{3}{4}n} \right] \tag{4.12}$$

$$= \sum_{n=-\infty}^{\infty} e^{-j2\pi nf_s t_0} \left[\frac{1}{2}\text{sinc}(\frac{1}{2}n)e^{-j2\pi\frac{1}{4}n} - \frac{1}{2}\text{sinc}(\frac{1}{2}n)e^{-j2\pi\frac{3}{4}n} \right] U(f_o - nf_s) \tag{4.13}$$

$$= \sum_{n=-\infty}^{\infty} \left[e^{-j2\pi nf_s t_0}(1 - e^{-j2\pi\frac{1}{2}n})\frac{1}{2}\text{sinc}(\frac{1}{2}n)e^{-j2\pi\frac{1}{4}n} \right] U(f_o - nf_s) \tag{4.14}$$

$$Y(f_o) = \sum_{n=-\infty}^{\infty} \left[\frac{e^{-j2\pi nf_s t_0}}{1 + j\frac{f_o}{f_{rc}}}(1 - e^{-j2\pi\frac{1}{2}n})\frac{1}{2}\text{sinc}(\frac{1}{2}n)e^{-j2\pi\frac{1}{4}n} \right] U(f_o - nf_s) \tag{4.15}$$

The resulting periodic transfer function is given in figure 4.4.

$$H_n(f_o) = \frac{e^{-j2\pi nf_s t_0}}{1 + j\frac{f_o}{f_{rc}}}(1 - e^{-j2\pi\frac{1}{2}n})\frac{1}{2}\text{sinc}(\frac{1}{2}n)e^{-j2\pi\frac{1}{4}n} \tag{4.16}$$

$$= \frac{e^{-j2\pi nf_s t_0}}{1 + j\frac{f_o}{f_{rc}}}(1 - e^{-j2\pi\frac{1}{2}n})\frac{1 - e^{-j2\pi\frac{1}{2}n}}{j2\pi n} \tag{4.17}$$

Note that $H_n(f_o)$ is decreasing with increasing n, resulting in a finite Noise Figure.

Figure 4.4: Switching Mixer Double Balanced H_n

4.2 Sampling Mixer

4.2.1 Single Balanced

The signal representation of the sampling mixer is shown in figure 4.5. The upper branch is a multiplication with a block wave, while the lower branch is a sampler followed by a hold filter. The two branches will be analyzed separately and joined later.

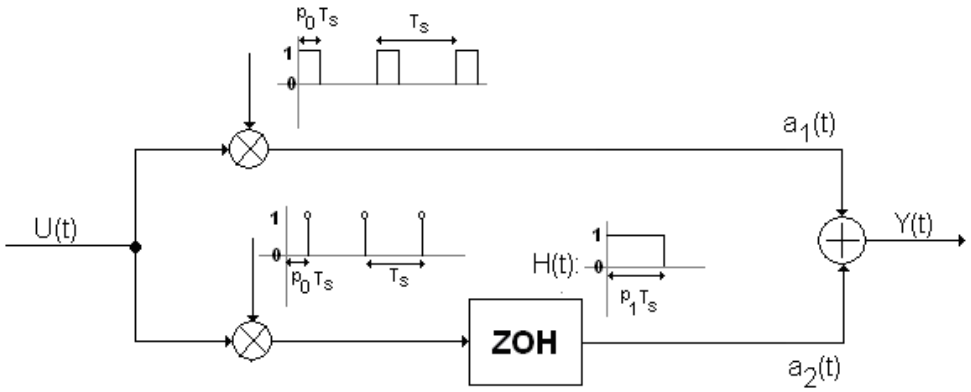

Figure 4.5: Single balanced sampling mixer signal representation

The time domain description of the upper branch is given by:

$$a_1(t) = u(t) \sum_{n=-\infty}^{\infty} \text{rect}(\frac{t-t_0}{p_0 T_s} - \frac{n}{p_0} - \frac{1}{2}) \tag{4.18}$$

$$= u(t) \sum_{n=-\infty}^{\infty} \text{rect}(\frac{t-t_0-nT_s-\frac{1}{2}p_0T_s}{p_0T_s}) \tag{4.19}$$

$$= u(t) \sum_{n=-\infty}^{\infty} p_0 \text{sinc}(p_0 n) e^{j2\pi n f_s (t-t_0-\frac{1}{2}p_0T_s)} \tag{4.20}$$

Transformation to the frequency domain gives:

$$A_1(f_o) = U(f_i) * \sum_{n=-\infty}^{\infty} p_0 \text{sinc}(p_0 n) e^{-j2\pi n f_s t_0} e^{-j2\pi \frac{1}{2} p_0 n} \delta(f_o - n f_s) \tag{4.21}$$

$$= \sum_{n=-\infty}^{\infty} e^{-j2\pi n f_s t_0} p_0 \text{sinc}(p_0 n) e^{-j2\pi \frac{1}{2} p_0 n} U(f_o - n f_s) \tag{4.22}$$

The time domain description of the lower branch is given by:

$$a_2(t) = \left[u(t) \sum_{n=-\infty}^{\infty} \delta(t - t_0 - nT_s - p_0 T_s) \right] * \text{rect}(\frac{t - \frac{1}{2}p_1 T_s}{p_1 T_s}) \tag{4.23}$$

Translation to the frequency domain gives:

$$A_2(f_o) = \left[U(f_i) * \sum_{n=-\infty}^{\infty} f_s \delta(f_o - n f_s) e^{-j2\pi n f_s t_0} e^{-j2\pi p_0 n} \right] p_1 T_s \text{sinc}(p_1 \frac{f_o}{f_s}) e^{-j2\pi \frac{1}{2} p_1 \frac{f_o}{f_s}} \tag{4.24}$$

$$= \sum_{n=-\infty}^{\infty} e^{-j2\pi n f_s t_0} p_1 \text{sinc}(p_1 \frac{f_o}{f_s}) e^{-j2\pi \frac{1}{2} p_1 \frac{f_o}{f_s}} e^{-j2\pi p_0 n} U(f_o - n f_s) \tag{4.25}$$

Resulting in a total response of:

$$Y(f_o) = A_1(f_o) + A_2(f_o) \tag{4.26}$$

$$= \sum_{n=-\infty}^{\infty} e^{-j2\pi n f_s t_0} \left[p_0 \text{sinc}(p_0 n) e^{-j2\pi \frac{1}{2} p_0 n} + p_1 \text{sinc}(p_1 \frac{f_o}{f_s}) e^{-j2\pi \frac{1}{2} p_1 \frac{f_o}{f_s}} e^{-j2\pi p_0 n} \right] U(f_o - n f_s) \tag{4.27}$$

$$= \sum_{n=-\infty}^{\infty} e^{-j2\pi n f_s t_0} \left[\frac{1 - e^{-j2\pi p_0 n}}{j2\pi n} + \frac{1 - e^{-j2\pi p_1 \frac{f_o}{f_s}}}{j2\pi \frac{f_o}{f_s}} e^{-j2\pi p_0 n} \right] U(f_o - n f_s) \tag{4.28}$$

The resulting periodic transfer function is given in figure 4.6.

$$H_n(f_o) = e^{-j2\pi n f_s t_0} \left[\frac{1 - e^{-j2\pi p_0 n}}{j2\pi n} + \frac{1 - e^{-j2\pi p_1 \frac{f_o}{f_s}}}{j2\pi \frac{f_o}{f_s}} e^{-j2\pi p_0 n} \right] \tag{4.29}$$

Or in sinc form:

$$H_n(f_o) = e^{-j2\pi n f_s t_0} \left[p_0 \text{sinc}(p_0 n) e^{-j2\pi \frac{p_0}{2} n} + p_1 \text{sinc}(p_1 \frac{f_o}{f_s}) e^{-j2\pi \frac{p_1}{2} \frac{f_o}{f_s}} e^{-j2\pi p_0 n} \right] \tag{4.30}$$

Note that the second part of this equation has a magnitude that does not depend on n, resulting in an infinite Noise Figure due to an infinite number of folding.

Figure 4.6: Sampling Mixer Single Balanced H_n

4.2.2 Double Balanced

The signal representation of the sampling mixer is shown in figure 4.7. There are four periodic phases: $p_0 = p_2$, $p_1 = p_3$, $p_0 + p_1 = \frac{1}{2}$, $p_2 + p_3 = \frac{1}{2}$. The analysis is similar to the single balanced case.

$$a_1(t) = u(t) \sum_{n=-\infty}^{\infty} \text{rect}(\frac{t - t_0 - nT_s - \frac{1}{2} p_0 T_s}{p_0 T_s}) \tag{4.31}$$

$$A_1(f_o) = \sum_{n=-\infty}^{\infty} e^{-j2\pi n f_s t_0} p_0 \text{sinc}(p_0 n) e^{-j2\pi \frac{1}{2} p_0 n} U(f_o - n f_s) \tag{4.32}$$

$$a_2(t) = \left[u(t) \sum_{n=-\infty}^{\infty} \delta(t - t_0 - nT_s - p_0 T_s) \right] * \text{rect}(\frac{t - \frac{1}{2} p_1 T_s}{p_1 T_s}) \tag{4.33}$$

$$A_2(f_o) = \sum_{n=-\infty}^{\infty} e^{-j2\pi n f_s t_0} p_1 \text{sinc}(p_1 \frac{f_o}{f_s}) e^{-j2\pi \frac{1}{2} p_1 \frac{f_o}{f_s}} e^{-j2\pi p_0 n} U(f_o - n f_s) \tag{4.34}$$

$$a_3(t) = -u(t) \sum_{n=-\infty}^{\infty} \text{rect}(\frac{t - t_2 - nT_s - \frac{1}{2} p_2 T_s}{p_2 T_s}) \tag{4.35}$$

$$A_3(f_o) = -\sum_{n=-\infty}^{\infty} e^{-j2\pi n f_s t_2} p_2 \text{sinc}(p_2 n) e^{-j2\pi \frac{1}{2} p_2 n} U(f_o - n f_s) \tag{4.36}$$

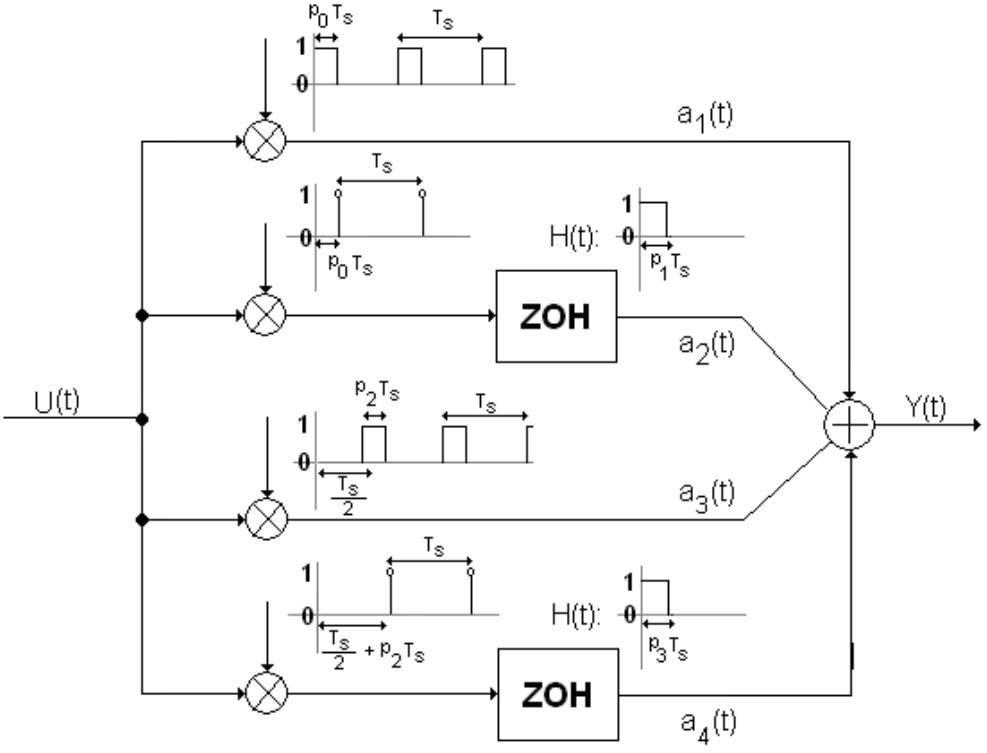

Figure 4.7: Double balanced sampling mixer signal representation

Because $p_0 = p_2$ and $t_2 = t_0 + \frac{1}{2}T_s$ this expression reduces to:

$$A_3(f_o) = -A_1(f_0)e^{-j2\pi\frac{1}{2}n} \tag{4.37}$$

$$a_4(t) = \left[-u(t)\sum_{n=-\infty}^{\infty}\delta(t - t_2 - nT_s - p_2T_s)\right] * \text{rect}(\frac{t - \frac{1}{2}p_3T_s}{p_3T_s}) \tag{4.38}$$

$$A_4(f_o) = -\sum_{n=-\infty}^{\infty} e^{-j2\pi nf_st_0}p_3\text{sinc}(p_3\frac{f_o}{f_s})e^{-j2\pi\frac{1}{2}p_3\frac{f_o}{f_s}}e^{-j2\pi p_2n}U(f_o - nf_s) \tag{4.39}$$

Because $p_1 = p_3$ and $t_2 = t_0 + \frac{1}{2}T_s$ this expression reduces to:

$$A_4(f_o) = -A_2(f_0)e^{-j2\pi\frac{1}{2}n} \tag{4.40}$$

Summing the four branches results in the total response:

$$Y(f_o) = A_1(f_o) + A_2(f_o) + A_3(f_o) + A_4(f_o) \tag{4.41}$$

$$\begin{aligned} &= \sum_{n=-\infty}^{\infty} e^{-j2\pi nf_st_0}(1 - e^{-j2\pi\frac{1}{2}n})\Big[p_0\text{sinc}(p_0n)e^{-j2\pi\frac{1}{2}p_0n} + \\ &\quad p_1\text{sinc}(p_1\frac{f_o}{f_s})e^{-j2\pi\frac{1}{2}p_1\frac{f_o}{f_s}}e^{-j2\pi p_0n}\Big]U(f_o - nf_s) \end{aligned} \tag{4.42}$$

$$= \sum_{n=-\infty}^{\infty} e^{-j2\pi n f_s t_0}(1 - e^{-j2\pi\frac{1}{2}n})\left[\frac{1 - e^{-j2\pi p_0 n}}{j2\pi n} + \frac{1 - e^{-j2\pi p_1 \frac{f_o}{f_s}}}{j2\pi\frac{f_o}{f_s}} e^{-j2\pi p_0 n}\right] U(f_o - nf_s) \quad (4.43)$$

The resulting periodic transfer function is given in figure 4.8.

$$H_n(f_o) = e^{-j2\pi n f_s t_0}(1 - e^{-j2\pi\frac{1}{2}n})\left[\frac{1 - e^{-j2\pi p_0 n}}{j2\pi n} + \frac{1 - e^{-j2\pi p_1 \frac{f_o}{f_s}}}{j2\pi\frac{f_o}{f_s}} e^{-j2\pi p_0 n}\right] \quad (4.44)$$

Or in sinc form:

$$H_n(f_o) = e^{-j2\pi n f_s t_0}(1 - e^{-j2\pi\frac{1}{2}n})\left[p_0 \text{sinc}(p_0 n) e^{-j2\pi\frac{p_0}{2}n} + p_1 \text{sinc}(p_1\frac{f_o}{f_s}) e^{-j2\pi\frac{p_1}{2}\frac{f_o}{f_s}} e^{-j2\pi p_0 n}\right] \quad (4.45)$$

Note that the second part of this equation has a magnitude that does not depend on n, resulting in an infinite Noise Figure due to an infinite number of folding.

Figure 4.8: Sampling Mixer Double Balanced H_n

4.3 Frequency Converter Model

4.3.1 Single Balanced

To calculate the frequency response of the LPTV network, equation 3.17 has to be evaluated, according to Strom and Signell [6]. In this case, $D = 2$ and the differential equations of the two phases are:

$$\begin{cases} \frac{dV_{out}(t)}{dt} = -\frac{1}{RC}V_{out}(t) + \frac{1}{RC}V_{in}(t) & , nT_s + t_0 < t < nT_s + t_1 \\ \frac{dV_{out}(t)}{dt} = 0 & , nT_s + t_1 < t < (n+1)T_s + t_0 \end{cases} \quad (4.46)$$

Instead of the RC time, it is more constructive using the cutoff frequency of the filter, defined as $f_{rc} = \frac{1}{2\pi RC}$. The derivation and evaluation of equation 3.13 is given in Appendix B, resulting in:

$$G(f_i) = \frac{e^{j2\pi p_0\frac{f_i}{f_s}} - e^{-2\pi p_0\frac{f_{rc}}{f_s}}}{e^{j2\pi\frac{f_i}{f_s}} - e^{-2\pi p_0\frac{f_{rc}}{f_s}}} \frac{1}{1 + j\frac{f_i}{f_{rc}}} \quad (4.47)$$

$$G_0(f_i) = G(f_i)e^{j2\pi f_i t_0} \quad (4.48)$$

$$G_1(f_i) = G(f_i)e^{j2\pi f_i t_2} \quad (4.49)$$

$$G_2(f_i) = G(f_i)e^{j2\pi f_i t_2} \quad (4.50)$$

$$(4.51)$$

The LTI response is easily calculated:

$$\text{phase0}\begin{cases} (j2\pi f_o I - A_1)^{-1} = \frac{1}{j2\pi f_o + 2\pi f_{rc}} = \frac{\frac{1}{2\pi f_{rc}}}{j\frac{f_o}{f_{rc}}+1} \\ B_1 = 2\pi f_{rc} \end{cases} \quad (4.52)$$

$$\text{phase1}\begin{cases} (j2\pi f_o I - A_2)^{-1} = \frac{1}{j2\pi f_o} \\ B_2 = 0 \end{cases} \quad (4.53)$$

Equation 3.17 is evaluated for phase 0:

$$X_0(f_o) = \sum_{n=-\infty}^{\infty} e^{-j2\pi n f_s t_0}(j2\pi f_o I - A_1)^{-1}\Bigg[B_1\frac{1-e^{-j2\pi np_0}}{j2\pi n} + f_s G_0(f_i)e^{-j2\pi f_i t_0} - f_s G_1(f_i)e^{-j2\pi f_i t_1}e^{-j2\pi np_0}\Bigg]U(f_i) \tag{4.54}$$

$$X_0(f_o) = \sum_{n=-\infty}^{\infty} e^{-j2\pi n f_s t_0}\Big(\frac{\frac{1}{2\pi f_{rc}}}{j\frac{f_o}{f_{rc}}+1}\Bigg[2\pi f_{rc}\frac{1-e^{-j2\pi np_0}}{j2\pi n} + f_s G(f_i)e^{j2\pi f_i t_0}e^{-j2\pi f_i t_0} - f_s G(f_i)e^{j2\pi f_i t_2}e^{-j2\pi f_i t_1}e^{-j2\pi np_0}\Bigg]U(f_i) \tag{4.55}$$

$$X_0(f_o) = \sum_{n=-\infty}^{\infty} e^{-j2\pi n f_s t_0}\Bigg[\frac{1}{1+j\frac{f_o}{f_{rc}}}\frac{1-e^{-j2\pi np_0}}{j2\pi n} + \frac{1-e^{j2\pi p_1\frac{f_i}{f_s}}e^{-j2\pi np_0}}{(2\pi\frac{f_{rc}}{f_s})(1+j\frac{f_o}{f_{rc}})}G(f_i)\Bigg]U(f_i) \tag{4.56}$$

Equation 3.17 is evaluated for phase 1:

$$X_1(f_0) = \sum_{n=-\infty}^{\infty} e^{-j2\pi n f_s t_1}(j2\pi f_o I - A_2)^{-1}\Bigg[B_2\frac{1-e^{-j2\pi np_1}}{j2\pi n} + f_s G_1(f_i)e^{-j2\pi f_i t_1} - f_s G_2(f_i)e^{-j2\pi f_i t_2}e^{-j2\pi np_1}\Bigg]U(f_i) \tag{4.57}$$

$$X_1(f_0) = \sum_{n=-\infty}^{\infty} e^{-j2\pi n f_s t_1}\frac{1}{j2\pi\frac{f_o}{f_s}}\Bigg[G(f_i)e^{j2\pi f_i t_2}e^{-j2\pi f_i t_1} - G(f_i)e^{j2\pi f_i t_2}e^{-j2\pi f_i t_2}e^{-j2\pi np_1}\Bigg]U(f_i) \tag{4.58}$$

$$X_1(f_o) = \sum_{n=-\infty}^{\infty} e^{-j2\pi n f_s t_1}\frac{1}{j2\pi\frac{f_o}{f_s}}G(f_i)(e^{j2\pi p_1\frac{f_i}{f_s}} - e^{-j2\pi p_1 n})U(f-nf_s) \tag{4.59}$$

$$= \sum_{n=-\infty}^{\infty} e^{-j2\pi n f_s t_1}\frac{1-e^{-j2\pi p_1\frac{f_o}{f_s}}}{j2\pi\frac{f_o}{f_s}}e^{j2\pi p_1\frac{f_i}{f_s}}G(f_i)U(f-nf_s) \tag{4.60}$$

$$= \sum_{n=-\infty}^{\infty} e^{-j2\pi n f_s t_0}\frac{1-e^{-j2\pi p_1\frac{f_o}{f_s}}}{j2\pi\frac{f_o}{f_s}}e^{-j2\pi p_0 n}e^{j2\pi p_1\frac{f_i}{f_s}}G(f_i)U(f-nf_s) \tag{4.61}$$

Summing these phase equations according to equation 3.11 gives the total response:

$$Y(f_0) = X(f_o) = X_0(f_o) + X_1(f_o) \tag{4.62}$$

$$= \sum_{n=-\infty}^{\infty} e^{-j2\pi n f_s t_0}\Bigg[\frac{1}{1+j\frac{f_o}{f_{rc}}}\frac{1-e^{-j2\pi p_0 n}}{j2\pi n} \tag{4.63}$$

$$+ \frac{1}{j2\pi\frac{f_o}{f_s}+2\pi\frac{f_{rc}}{f_s}}(1-e^{j2\pi p_1\frac{f_i}{f_s}}e^{-j2\pi p_0 n})G(f_i) \tag{4.64}$$

$$+ \frac{1-e^{-j2\pi p_1\frac{f_o}{f_s}}}{j2\pi\frac{f_o}{f_s}}e^{-j2\pi p_0 n}e^{j2\pi p_1\frac{f_o}{f_s}}G(f_i)\Bigg]U(f_i) \tag{4.65}$$

Since the state variable X is also the output: $Y(f_0) = X(f_o)$. Then the periodic transfer function becomes:

$$H_n(f_o) = e^{-j2\pi n f_s t_0}\Bigg[\underbrace{\frac{1}{1+j\frac{f_o}{f_{rc}}}\frac{1-e^{-j2\pi p_0 n}}{j2\pi n}}_{partB} + \underbrace{\frac{1}{(2\pi\frac{f_{rc}}{f_s})(1+j\frac{f_o}{f_{rc}})}(1-e^{j2\pi p_1\frac{f_i}{f_s}}e^{-j2\pi p_0 n})G(f_i)}_{partC} + \underbrace{\frac{1-e^{-j2\pi p_1\frac{f_o}{f_s}}}{j2\pi\frac{f_o}{f_s}}e^{-j2\pi p_0 n}G(f_i)e^{j2\pi p_1\frac{f_i}{f_s}}}_{partD}\Bigg] \tag{4.66}$$

Part B and part C of this equation both have the factor $\frac{1}{1+j\frac{f_o}{f_{rc}}}$, but part D does not. In order to split off this common factor, part D is multiplied by the unity factor $\frac{1+j\frac{f_o}{f_{rc}}}{1+j\frac{f_o}{f_{rc}}}$:

$$H_n(f_o) = e^{-j2\pi n f_s t_0}(1-e^{-j2\pi\frac{1}{2}n})\frac{1}{1+j\frac{f_o}{f_{rc}}}\Bigg[\frac{1-e^{-j2\pi p_0 n}}{j2\pi n} + \frac{1-e^{-j2\pi p_1\frac{f_o}{f_s}}}{j2\pi\frac{f_o}{f_s}}e^{-j2\pi p_0 n}G(f_i)e^{j2\pi p_1\frac{f_i}{f_s}} + \frac{1}{2\pi\frac{f_{rc}}{f_s}}(1-e^{j2\pi p_1\frac{f_i}{f_s}}e^{-j2\pi p_0 n})G(f_i) - \frac{j\frac{f_o}{f_{rc}}}{j2\pi\frac{f_o}{f_s}}(1-e^{-j2\pi p_1\frac{f_o}{f_s}})e^{-j2\pi p_0 n}G(f_i)e^{j2\pi p_1\frac{f_i}{f_s}}\Bigg] \tag{4.67}$$

The lower line now has similar factors and can be simplified further:

$$H_n(f_o) = e^{-j2\pi n f_s t_0}(1-e^{-j2\pi\frac{1}{2}n})\frac{1}{1+j\frac{f_o}{f_{rc}}}\Bigg[\frac{1-e^{-j2\pi p_0 n}}{j2\pi n} + \frac{1-e^{-j2\pi p_1\frac{f_o}{f_s}}}{j2\pi\frac{f_o}{f_s}}e^{-j2\pi p_0 n}G(f_i)e^{j2\pi p_1\frac{f_i}{f_s}} + \frac{G(f_i)}{2\pi\frac{f_{rc}}{f_s}}\underbrace{\left(1-e^{j2\pi p_1\frac{f_i}{f_s}}e^{-j2\pi p_0 n}+e^{j2\pi p_1\frac{f_i}{f_s}}e^{-j2\pi p_0 n}-e^{-j2\pi n}\right)}_{partE}\Bigg] \tag{4.68}$$

Part E evaluates to $(1-e^{-j2\pi n}) = 0$. The resulting periodic transfer function is given in figure 4.9.

$$H_n(f_o) = e^{-j2\pi n f_s t_0} \frac{1}{1 + j\frac{f_o}{f_{rc}}} \left[\frac{1 - e^{-j2\pi p_0 n}}{j2\pi n} + \frac{1 - e^{-j2\pi p_1 \frac{f_o}{f_s}}}{j2\pi \frac{f_o}{f_s}} e^{-j2\pi p_0 n} G(f_i) e^{j2\pi p_1 \frac{f_i}{f_s}} \right] \tag{4.69}$$

Or in sincform:

$$\begin{aligned} H_n(f_o) = e^{-j2\pi n f_s t_0} \frac{1}{1 + j\frac{f_o}{f_{rc}}} \cdot \\ \left[p_0 \cdot \mathrm{sinc}(p_0 n) e^{-j2\pi \frac{p_0}{2} n} + p_1 \cdot \mathrm{sinc}(p_1 \frac{f_o}{f_s}) e^{-j2\pi \frac{p_1}{2} \frac{f_o}{f_s}} e^{-j2\pi p_0 n} G(f_i) e^{j2\pi p_1 \frac{f_i}{f_s}} \right] \end{aligned} \tag{4.70}$$

Given that:

$$G(f_i) = \frac{e^{j2\pi p_0 \frac{f_i}{f_s}} - e^{-2\pi p_0 \frac{f_{rc}}{f_s}}}{e^{j2\pi \frac{f_i}{f_s}} - e^{-2\pi p_0 \frac{f_{rc}}{f_s}}} \frac{1}{1 + j\frac{f_i}{f_{rc}}} \tag{4.71}$$

Figure 4.9: Frequency Converter Model Single Balanced H_n

4.3.2 Double Balanced

The double balanced frequency converter model is similar to the single balanced version, but with the double amount of periodic phases. There are four phases so $D = 4$ and the balancing forces the relationships:

$$p_0 = p_2,\ p_1 = p_3,\ p_0 + p_1 = \frac{1}{2},\ p_2 + p_3 = \frac{1}{2} \tag{4.72}$$

During phase 0 and phase 2 the circuit is a RC filter and during phase 1 and phase 3 the voltage on the capacitors remains static. Therefore the differential equations are given by:

$$\begin{cases} RC\frac{dV_{out}(t)}{dt} + V_{out}(t) = V_{in}(t) & , t_0 + nT_s < t < t1 + nT_s \\ V_{out}(t) = V_{out}(nT_s + t_1) & , t_1 + nT_s < t < t2 + nT_s \\ RC\frac{dV_{out}(t)}{dt} + V_{out}(t) = -V_{in}(t) & , t_2 + nT_s < t < t3 + nT_s \\ V_{out}(t) = V_{out}(nT_s + t_3) & , t_3 + nT_s < t < t0 + (n+1)T_s \end{cases} \tag{4.73}$$

The derivation of the difference equation 3.12 is given in appendix B. The resulting equations for $G_k(f_i)$ are:

$$G(f_i) = -\frac{e^{j2\pi p_0 \frac{f_i}{f_s}} - e^{-2\pi p_0 \frac{f_{rc}}{f_s}}}{e^{j2\pi \frac{1}{2} \frac{f_i}{f_s}} + e^{-2\pi p_0 \frac{f_{rc}}{f_s}}} \frac{1}{1 + j\frac{f_i}{f_{rc}}} \tag{4.74}$$

$$G_0(f_i) = G(f_i) e^{j2\pi f_i t_0} \tag{4.75}$$

$$G_1(f_i) = -G(f_i) e^{j2\pi f_i t_2} \tag{4.76}$$

$$G_2(f_i) = -G(f_i) e^{j2\pi f_i t_2} \tag{4.77}$$

$$G_3(f_i) = G(f_i) e^{j2\pi f_i t_4} \tag{4.78}$$

$$G_4(f_i) = G(f_i) e^{j2\pi f_i t_4} \tag{4.79}$$

The solution to the differential equations in each phase is trivial:

$$\text{phase0,phase2}\begin{cases}(j2\pi f_o I - A_1)^{-1} = (j2\pi f_o I - A_3)^{-1} = \frac{1}{j2\pi f_o + 2\pi f_{rc}} = \frac{\frac{1}{2\pi f_{rc}}}{j\frac{f_o}{f_{rc}}+1} \\ B_1 = B_3 = 2\pi f_{rc}\end{cases} \tag{4.80}$$

$$\text{phase1,phase3}\begin{cases}(j2\pi f_o I - A_2)^{-1} = (j2\pi f_o I - A_4)^{-1} = \frac{1}{j2\pi f_o} \\ B_2 = B_4 = 0\end{cases} \tag{4.81}$$

Equation 3.17 is evaluated for phase 0:

$$\begin{aligned}X_0(f_o) = \sum_{n=-\infty}^{\infty} e^{-j2\pi n f_s t_0}(j2\pi f_o I - A_1)^{-1}\Big[B_1\frac{1-e^{-j2\pi np_0}}{j2\pi n} \\ + f_s G_0(f_i)e^{-j2\pi f_i t_0} - f_s G_1(f_i)e^{-j2\pi f_i t_1}e^{-j2\pi np_0}\Big]U(f_i)\end{aligned} \tag{4.82}$$

$$\begin{aligned}X_0(f_o) = \sum_{n=-\infty}^{\infty} e^{-j2\pi n f_s t_0}(\frac{\frac{1}{2\pi f_{rc}}}{j\frac{f_o}{f_{rc}}+1}\Big[2\pi f_{rc}\frac{1-e^{-j2\pi np_0}}{j2\pi n} \\ + f_s G(f_i)e^{j2\pi f_i t_0}e^{-j2\pi f_i t_0} + f_s G(f_i)e^{j2\pi f_i t_2}e^{-j2\pi f_i t_1}e^{-j2\pi np_0}\Big]U(f_i)\end{aligned} \tag{4.83}$$

$$X_0(f_o) = \sum_{n=-\infty}^{\infty} e^{-j2\pi n f_s t_0}\Big[\frac{1}{1+j\frac{f_o}{f_{rc}}}\frac{1-e^{-j2\pi np_0}}{j2\pi n} + \frac{1+e^{j2\pi p_1\frac{f_i}{f_s}}e^{-j2\pi np_0}}{(2\pi\frac{f_{rc}}{f_s})(1+j\frac{f_o}{f_{rc}})}G(f_i)\Big]U(f_i) \tag{4.84}$$

Equation 3.17 is evaluated for phase 2:

$$\begin{aligned}X_2(f_o) = \sum_{n=-\infty}^{\infty} e^{-j2\pi n f_s t_2}(j2\pi f_o I - A_3)^{-1}\Big[B_3\frac{1-e^{-j2\pi np_2}}{j2\pi n} \\ + f_s G_2(f_i)e^{-j2\pi f_i t_2} - f_s G_3(f_i)e^{-j2\pi f_i t_3}e^{-j2\pi np_2}\Big]U(f_i)\end{aligned} \tag{4.85}$$

$$\begin{aligned}X_2(f_o) = \sum_{n=-\infty}^{\infty} e^{-j2\pi n f_s t_0}e^{-j2\pi\frac{1}{2}n}(\frac{\frac{1}{2\pi f_{rc}}}{j\frac{f_o}{f_{rc}}+1}\Big[-2\pi f_{rc}\frac{1-e^{-j2\pi np_2}}{j2\pi n} \\ - f_s G(f_i)e^{j2\pi f_i t_2}e^{-j2\pi f_i t_2} - f_s G(f_i)e^{j2\pi f_i t_4}e^{-j2\pi f_i t_3}e^{-j2\pi np_2}\Big]U(f_i)\end{aligned} \tag{4.86}$$

$$X_2(f_o) = \sum_{n=-\infty}^{\infty} -e^{-j2\pi n f_s t_0}e^{-j2\pi\frac{1}{2}n}\Big[\frac{1}{1+j\frac{f_o}{f_{rc}}}\frac{1-e^{-j2\pi np_2}}{j2\pi n} + \frac{1+e^{j2\pi p_3\frac{f_i}{f_s}}e^{-j2\pi p_2 n}}{(2\pi\frac{f_{rc}}{f_s})(1+j\frac{f_o}{f_{rc}})}G_0(f_i)\Big]U(f_i) \tag{4.87}$$

Inspection reveals that $X_2(f_o) = -X_0(f_o)e^{j2\pi\frac{1}{2}n}$.Equation 3.17 is evaluated for phase 1:

$$X_1(f_0) = \sum_{n=-\infty}^{\infty} e^{-j2\pi n f_s t_1}(j2\pi f_o I - A_2)^{-1}\Bigg[B_2\frac{1-e^{-j2\pi np_1}}{j2\pi n} + f_s G_1(f_i)e^{-j2\pi f_i t_1} - f_s G_2(f_i)e^{-j2\pi f_i t_2}e^{-j2\pi np_1}\Bigg]U(f_i) \tag{4.88}$$

$$X_1(f_0) = \sum_{n=-\infty}^{\infty} e^{-j2\pi n f_s t_1}\frac{1}{j2\pi\frac{f_o}{f_s}} \Big[-G(f_i)e^{j2\pi f_i t_2}e^{-j2\pi f_i t_1} + G(f_i)e^{j2\pi f_i t_2}e^{-j2\pi f_i t_2}e^{-j2\pi np_1}\Big]U(f_i) \tag{4.89}$$

$$X_1(f_o) = \sum_{n=-\infty}^{\infty} -e^{-j2\pi n f_s t_1}\frac{1}{j2\pi\frac{f_o}{f_s}}G(f_i)(e^{j2\pi p_1\frac{f_i}{f_s}} - e^{-j2\pi p_1 n})U(f-nf_s) \tag{4.90}$$

$$= \sum_{n=-\infty}^{\infty} -e^{-j2\pi n f_s t_1}\frac{1-e^{-j2\pi p_1\frac{f_o}{f_s}}}{j2\pi\frac{f_o}{f_s}}e^{j2\pi p_1\frac{f_i}{f_s}}G(f_i)U(f-nf_s) \tag{4.91}$$

$$= \sum_{n=-\infty}^{\infty} -e^{-j2\pi n f_s t_0}\frac{1-e^{-j2\pi p_1\frac{f_o}{f_s}}}{j2\pi\frac{f_o}{f_s}}e^{-j2\pi p_0 n}e^{j2\pi p_1\frac{f_i}{f_s}}G(f_i)U(f-nf_s) \tag{4.92}$$

Equation 3.17 is evaluated for phase 3:

$$X_3(f_0) = \sum_{n=-\infty}^{\infty} e^{-j2\pi n f_s t_3}(j2\pi f_o I - A_4)^{-1}\Bigg[B_4\frac{1-e^{-j2\pi nh_3}}{j2\pi n} + f_s G_3(f_i)e^{-j2\pi f_i t_3} - f_s G_4(f_i)e^{-j2\pi f_i t_4}e^{-j2\pi np_3}\Bigg]U(f_i) \tag{4.93}$$

$$X_3(f_0) = \sum_{n=-\infty}^{\infty} e^{-j2\pi n f_s t_1}e^{-j2\pi\frac{1}{2}n}\frac{1}{j2\pi\frac{f_o}{f_s}} \Big[-G(f_i)e^{j2\pi f_i t_4}e^{-j2\pi f_i t_3} + G(f_i)e^{j2\pi f_i t_4}e^{-j2\pi f_i t_4}e^{-j2\pi np_3}\Big]U(f_i) \tag{4.94}$$

$$X_3(f_o) = \sum_{n=-\infty}^{\infty} -e^{-j2\pi n f_s t_1}e^{-j2\pi\frac{1}{2}n}\frac{1}{j2\pi\frac{f_o}{f_s}}G(f_i)(e^{j2\pi p_3\frac{f_i}{f_s}} - e^{-j2\pi np_3})U(f-nf_s) \tag{4.95}$$

$$= \sum_{n=-\infty}^{\infty} -e^{-j2\pi n f_s t_1}e^{-j2\pi\frac{1}{2}n}\frac{1-e^{-j2\pi p_3\frac{f_o}{f_s}}}{j2\pi\frac{f_o}{f_s}}G(f_i)e^{j2\pi p_3\frac{f_i}{f_s}}U(f-nf_s) \tag{4.96}$$

$$= \sum_{n=-\infty}^{\infty} -e^{-j2\pi n f_s t_0}e^{-j2\pi\frac{1}{2}n}\frac{1-e^{-j2\pi p_3\frac{f_o}{f_s}}}{j2\pi\frac{f_o}{f_s}}e^{-j2\pi p_0 n}G(f_i)e^{j2\pi p_3\frac{f_i}{f_s}}U(f-nf_s) \tag{4.97}$$

$$\tag{4.98}$$

Inspection reveals that $X_3(f_o) = -X_1(f_o)e^{j2\pi\frac{1}{2}n}$. Summing these phase equations according to equation 3.11 gives the total response:

$$Y(f_0) = X(f_o) = X_0(f_o) + X_1(f_o) + X_2(f_o) + X_3(f_o) \tag{4.99}$$

$$= \sum_{n=-\infty}^{\infty} e^{-j2\pi n f_s t_0}(1 - e^{j2\pi\frac{1}{2}n})\left[\frac{1}{1+j\frac{f_o}{f_{rc}}}\frac{1-e^{-j2\pi p_0 n}}{j2\pi n}\right. \tag{4.100}$$

$$+ \frac{1}{j2\pi\frac{f_o}{f_s} + 2\pi\frac{f_{rc}}{f_s}}(1 + e^{j2\pi p_1\frac{f_i}{f_s}}e^{-j2\pi p_0 n})G(f_i) \tag{4.101}$$

$$\left. - \frac{1-e^{-j2\pi p_1\frac{f_o}{f_s}}}{j2\pi\frac{f_o}{f_s}}e^{-j2\pi p_0 n}e^{j2\pi p_1\frac{f_o}{f_s}}G(f_i)\right]U(f_i) \tag{4.102}$$

Since the state variable X is also the output: $Y(f_0) = X(f_o)$. Then the periodic transfer function becomes:

$$\begin{aligned} H_n(f_o) =& e^{-j2\pi n f_s t_0}\underbrace{(1 - e^{-j2\pi\frac{1}{2}n})}_{partA}\left[\underbrace{\frac{1}{1+j\frac{f_o}{f_{rc}}}\frac{1-e^{-j2\pi p_0 n}}{j2\pi n}}_{partB}\right. \\ &\left. + \underbrace{\frac{1}{(2\pi\frac{f_{rc}}{f_s})(1+j\frac{f_o}{f_{rc}})}(1 + e^{j2\pi p_1\frac{f_i}{f_s}}e^{-j2\pi p_0 n})G(f_i)}_{partC} - \underbrace{\frac{1-e^{-j2\pi p_1\frac{f_o}{f_s}}}{j2\pi\frac{f_o}{f_s}}e^{-j2\pi p_0 n}G(f_i)e^{j2\pi p_1\frac{f_i}{f_s}}}_{partD}\right] \end{aligned} \tag{4.103}$$

Part B and part C of this equation both have the factor $\frac{1}{1+j\frac{f_o}{f_{rc}}}$, but part D does not. In order to split off this common factor, part D is multiplied by the unity factor $\frac{1+j\frac{f_o}{f_{rc}}}{1+j\frac{f_o}{f_{rc}}}$:

$$\begin{aligned} H_n(f_o) =& e^{-j2\pi n f_s t_0}(1 - e^{-j2\pi\frac{1}{2}n})\frac{1}{1+j\frac{f_o}{f_{rc}}}\left[\frac{1-e^{-j2\pi p_0 n}}{j2\pi n} + \frac{1-e^{-j2\pi p_1\frac{f_o}{f_s}}}{j2\pi\frac{f_o}{f_s}}e^{-j2\pi p_0 n}G(f_i)e^{j2\pi p_1\frac{f_i}{f_s}}\right. \\ &\left. + \frac{1}{2\pi\frac{f_{rc}}{f_s}}(1 + e^{j2\pi p_1\frac{f_i}{f_s}}e^{-j2\pi p_0 n})G(f_i) - \frac{j\frac{f_o}{f_{rc}}}{j2\pi\frac{f_o}{f_s}}(1 - e^{-j2\pi p_1\frac{f_o}{f_s}})e^{-j2\pi p_0 n}G(f_i)e^{j2\pi p_1\frac{f_i}{f_s}}\right] \end{aligned} \tag{4.104}$$

The lower line now has similar factors and can be simplified further:

$$\begin{aligned} H_n(f_o) =& e^{-j2\pi n f_s t_0}(1 - e^{-j2\pi\frac{1}{2}n})\frac{1}{1+j\frac{f_o}{f_{rc}}}\left[\frac{1-e^{-j2\pi p_0 n}}{j2\pi n} + \frac{1-e^{-j2\pi p_1\frac{f_o}{f_s}}}{j2\pi\frac{f_o}{f_s}}e^{-j2\pi p_0 n}G(f_i)e^{j2\pi p_1\frac{f_i}{f_s}}\right. \\ &\left. + \frac{G(f_i)}{2\pi\frac{f_{rc}}{f_s}}\underbrace{\left(1 + e^{j2\pi p_1\frac{f_i}{f_s}}e^{-j2\pi p_0 n} - e^{j2\pi p_1\frac{f_i}{f_s}}e^{-j2\pi p_0 n} + e^{-j2\pi\frac{1}{2}n}\right)}_{partE}\right] \end{aligned} \tag{4.105}$$

Part E evaluates to $(1 + e^{-j2\pi\frac{1}{2}n})$ which multiplied by part A gives zero:

$$(1 - e^{-j2\pi\frac{1}{2}n})(1 + e^{-j2\pi\frac{1}{2}n}) = 1 - e^{-j2\pi n} = 1 - 1 = 0 \tag{4.106}$$

The resulting periodic transfer function is given in figure 4.10.

$$H_n(f_o) = e^{-j2\pi n f_s t_0}(1 - e^{-j2\pi\frac{1}{2}n})\frac{1}{1 + j\frac{f_o}{f_{rc}}} \cdot \left[\frac{1 - e^{-j2\pi p_0 n}}{j2\pi n} - \frac{1 - e^{-j2\pi p_1\frac{f_o}{f_s}}}{j2\pi\frac{f_o}{f_s}} e^{-j2\pi p_0 n} G(f_i) e^{j2\pi p_1\frac{f_i}{f_s}}\right] \tag{4.107}$$

Or in sincform:

$$H_n(f_o) = e^{-j2\pi n f_s t_0}(1 - e^{-j2\pi\frac{1}{2}n})\frac{1}{1 + j\frac{f_o}{f_{rc}}} \cdot \left[p_0 \cdot \mathrm{sinc}(p_0 n) e^{-j2\pi\frac{p_0}{2}n} - p_1 \cdot \mathrm{sinc}(p_1\frac{f_o}{f_s}) e^{-j2\pi\frac{p_1}{2}\frac{f_o}{f_s}} e^{-j2\pi p_0 n} G(f_i) e^{j2\pi p_1\frac{f_i}{f_s}}\right] \tag{4.108}$$

Given that:

$$G(f_i) = -\frac{e^{j2\pi p_0\frac{f_i}{f_s}} - e^{-2\pi p_0\frac{f_{rc}}{f_s}}}{e^{j2\pi\frac{1}{2}\frac{f_i}{f_s}} + e^{-2\pi p_0\frac{f_{rc}}{f_s}}} \frac{1}{1 + j\frac{f_i}{f_{rc}}} \tag{4.109}$$

Figure 4.10: Frequency Converter Model Double Balanced H_n

4.4 Summary

The periodic transfer function of a switching mixer and sampling mixer can be calculated using the definition of the periodic transfer function and Fourier frequency domain identities. However, the memory effect of the frequency converter model prevents a similar approach and instead the full Strom and Signell theory has to be used.

For all three mixer types the periodic transfer functions were derived for both the single balanced en double balanced case. The double balanced transfer functions differ mainly from the single balanced ones by an additional factor $(1 - e^{-j2\pi\frac{1}{2}n})$, resulting in all even order harmonics to be zero. The same result was derived from Strom and Signell theory in section 3.3.4.

Chapter 5

Mixer Parameter Exploration

In this chapter the expressions for the double balanced frequency converter model are examined further. The goal is to derive simpler expressions for important performance figures like conversion gain and noise figure. The periodic transfer function is repeated here for convenience:

$$H_n(f_o) = e^{-j2\pi n f_s t_0}(1 - e^{-j2\pi\frac{1}{2}n})\frac{1}{1+j\frac{f_o}{f_{rc}}}\cdot \left[\underbrace{\frac{1-e^{-j2\pi p_0 n}}{j2\pi n}}_{partA} - \underbrace{\frac{1-e^{-j2\pi p_1\frac{f_o}{f_s}}}{j2\pi\frac{f_o}{f_s}}e^{-j2\pi p_o n}G(f_i)e^{j2\pi p_1\frac{f_i}{f_s}}}_{partB}\right] \tag{5.1}$$

Given that:

$$G(f_i) = -\frac{e^{j2\pi p_0\frac{f_i}{f_s}} - e^{-2\pi p_0\frac{f_{rc}}{f_s}}}{e^{j2\pi\frac{1}{2}\frac{f_i}{f_s}} + e^{-2\pi p_0\frac{f_{rc}}{f_s}}}\frac{1}{1+j\frac{f_i}{f_{rc}}} \tag{5.2}$$

5.1 Parameter Sweep

By choosing special values for the duty cycle p_0 and the bandwidth f_{rc} equation 5.1 can be simplified.

5.1.1 Duty Cycle

Put the duty cycle to 50 percent, which is $p_0 = \frac{1}{2}$ and $p_1 = 0$. Part B now is zero because $1 - e^{-j2\pi p_1\frac{f_o}{f_s}} = 1 - e^0 = 0$ and only part A remains:

$$H_n(f_o) = e^{-j2\pi n f_s t_0}(1 - e^{-j2\pi\frac{1}{2}n})\frac{1}{1+j\frac{f_o}{f_{rc}}}\frac{1-e^{-j2\pi\frac{1}{2}n}}{j2\pi n} \tag{5.3}$$

Which is the expression for the double balanced switching mixer (figure 4.4).

5.1.2 RC frequency

First the effect of choosing an infinitely large f_{rc} on the periodic transfer function of the double balanced Tayloe mixer is considered.

For $G(f_i)$ the limit is:

$$G(f_i) = -\frac{e^{j2\pi p_0 \frac{f_i}{f_s}} - e^{-\infty}}{e^{j2\pi \frac{1}{2} \frac{f_i}{f_s}} + e^{-\infty}} \frac{1}{1} \tag{5.4}$$

$$= -e^{j2\pi p_0 \frac{f_i}{f_s}} e^{-j2\pi \frac{1}{2} \frac{f_i}{f_s}} \tag{5.5}$$

The periodic transfer function becomes:

$$H_n(f_o) = e^{-j2\pi n f_s t_0}(1 - e^{-j2\pi \frac{1}{2} n})[\frac{1 - e^{-j2\pi p_0 n}}{j2\pi n} + \frac{1 - e^{-j2\pi p_1 \frac{f_o}{f_s}}}{j2\pi \frac{f_o}{f_s}} e^{-j2\pi p_0 \frac{f_o}{f_s}} e^{j2\pi p_0 \frac{f_i}{f_s}}] \tag{5.6}$$

$$= e^{-j2\pi n f_s t_0}(1 - e^{-j2\pi \frac{1}{2} n})[\frac{1 - e^{-j2\pi p_0 n}}{j2\pi n} + \frac{1 - e^{-j2\pi p_1 \frac{f_o}{f_s}}}{j2\pi \frac{f_o}{f_s}} e^{-j2\pi p_0 n}] \tag{5.7}$$

Which is the expression for the double balanced sampling mixer (figure 4.8). Now make the duty cycle very small so that $p_0 \cong 0$ and $p_1 = \frac{1}{2}$ then the expression becomes:

$$H_n(f_o) = e^{-j2\pi n f_s t_0}(1 - e^{-j2\pi \frac{1}{2} n}) \frac{1 - e^{-j2\pi \frac{1}{2} \frac{f_o}{f_s}}}{j2\pi \frac{f_o}{f_s}} \tag{5.8}$$

Which is the expression for a double balanced sampler with zero-order-hold.

5.1.3 The big picture

The previous two subsections have proved that equation 5.1 describes all the mixer types discussed in Chapter 2 and that different mixer forms arise from different values of the duty cycle p_0 and bandwidth f_{rc}. Table 5.1 summarizes the conclusions made.

Table 5.1: Frequency Converter Parameter Variation

	$f_{rc} = \infty$	$f_{rc} < f_s$
$p_0 = \frac{1}{2}$		switching mixer
$p_0 = \frac{1}{4}$		Tayloe mixer
$0 < p_0 < \frac{1}{2}$	sampling mixer	
$p_0 \approx 0$	sampler + zero-order-hold	

5.2 Approximations

The equation for G is simplified when two conditions are assumed:

- Only the behavior around DC output frequency is concerned: $f_0 = 0$ and $f_i = nf_s$
- The bandwidth is small with respect to the sampling frequency: $f_{rc} < 0.1 \cdot f_s$

Substituting the first condition into equation 5.2 result in:

$$G(f_i) = -\frac{e^{j2\pi p_0 n} - e^{-2\pi p_0 \frac{f_{rc}}{f_s}}}{e^{j2\pi \frac{1}{2} n} + e^{-2\pi p_0 \frac{f_{rc}}{f_s}}} \frac{1}{1 + j\frac{2\pi p_0 n}{2\pi p_0 \frac{f_{rc}}{f_s}}} \tag{5.9}$$

$$= \frac{2\pi p_0 \frac{f_{rc}}{f_s}}{1 - e^{-2\pi p_0 \frac{f_{rc}}{f_s}}} \frac{e^{j2\pi p_0 n} - e^{-2\pi p_0 \frac{f_{rc}}{f_s}}}{2\pi p_0 \frac{f_{rc}}{f_s} + j2\pi p_0 n} \tag{5.10}$$

hen taking the limit from f_{rc} toward zero to apply the second condition:

$$\lim_{f_{rc}\to 0}[\frac{2\pi p_0 \frac{f_{rc}}{f_s}}{1 - e^{-2\pi p_0 \frac{f_{rc}}{f_s}}} \frac{e^{j2\pi p_0 n} - e^{-2\pi p_0 \frac{f_{rc}}{f_s}}}{2\pi p_0 \frac{f_{rc}}{f_s} + j2\pi p_0 n}] = \tag{5.11}$$

$$\lim_{f_{rc}\to 0}[\frac{2\pi p_0 \frac{f_{rc}}{f_s}}{1 - e^{-2\pi p_0 \frac{f_{rc}}{f_s}}}] \cdot \lim_{f_{rc}\to 0}[\frac{e^{-j2\pi p_0 n} - e^{-2\pi p_0 \frac{f_{rc}}{f_s}}}{2\pi p_0 \frac{f_{rc}}{f_s} + j2\pi p_0 n}] = \tag{5.12}$$

$$1 \cdot \frac{e^{j2\pi p_0 n} - 1}{j2\pi p_0 n} \tag{5.13}$$

Entering this resulting formula for G into part B of equation 5.1 gives:

$$\frac{1 - e^{-j2\pi p_1 \frac{f_o}{f_s}}}{j2\pi \frac{f_o}{f_s}} e^{-j2\pi p_o \frac{f_o}{f_s}} \frac{e^{-j2\pi p_0 n} - 1}{j2\pi p_0 n} e^{j2\pi \frac{1}{2} \frac{f_i}{f_s}} = \tag{5.14}$$

$$-p_1 \frac{e^{-j2\pi p_0 n} - 1}{j2\pi p_0 n} \tag{5.15}$$

Which gives for the total periodic transfer function:

$$H_n(f_o) = e^{-j2\pi n f_s t_0}(1 - e^{-j2\pi \frac{1}{2} n}) \frac{1}{1 + j\frac{f_o}{f_{rc}}} [\frac{1 - e^{-j2\pi p_0 n}}{j2\pi n} + p_1 \frac{e^{-j2\pi p_0 n} - 1}{j2\pi p_0 n}] \tag{5.16}$$

$$= e^{-j2\pi n f_s t_0}(1 - e^{-j2\pi \frac{1}{2} n})(p_0 + p_1) \frac{e^{-j2\pi p_0 n} - 1}{j2\pi p_0 n} \tag{5.17}$$

$$= e^{-j2\pi n f_s t_0} \frac{(1 - e^{-j2\pi \frac{1}{2} n})}{2} \mathrm{sinc}(p_0 n) e^{-j2\pi \frac{p_0}{2} n} \tag{5.18}$$

This expression is only valid for narrow band operation and for $f_o \approx 0$. The magnitude is equal to $\mathrm{sinc}(p_0 n)$ for odd n and zero for even n. Using this result, the conversion gain is estimated as $\mathrm{sinc}(p_0)$ and the noise figure is estimated as:

$$NF(0Hz) = 10 \log(\frac{\sum_{n=odd} \mathrm{sinc}(p_0 n)^2}{\mathrm{sinc}(p_0)^2}) \tag{5.19}$$

Evaluations of this equation and equation 5.1 show that the estimate for the noise figure is also valid for $f_0 < f_s$. Figure 5.1 show these expressions evaluated for some values of p_0. The case where $p_0 = \frac{1}{4}$ gives the best balance between low conversion loss and low noise figure.

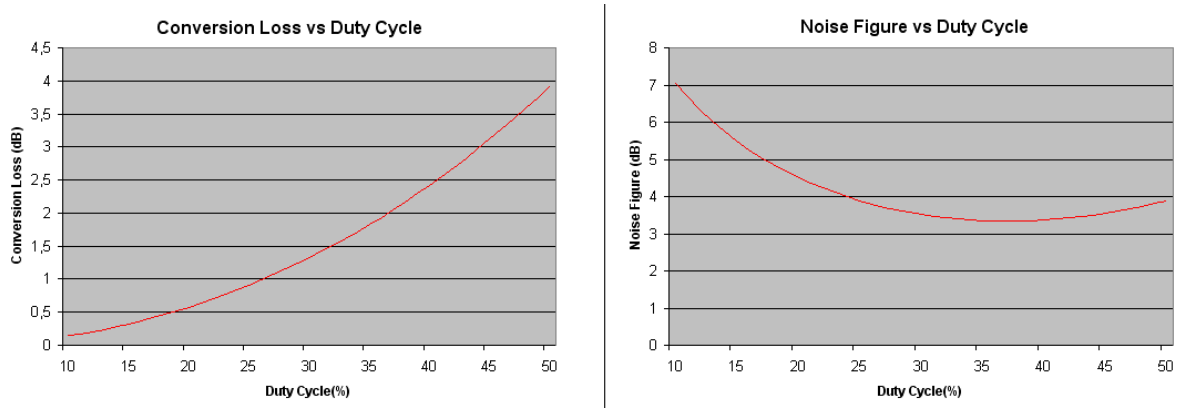

Figure 5.1: Approximate Conversion Loss and Noise Figure

The question arises if this approximation can be extended for output frequencies higher then DC. Evaluations of equation 5.1 show that by adding the term $\frac{1}{1+j\frac{f_o}{2p_0 f_{rc}}}$ the approximation is very good for $f_o < f_s$. This extra term then determines the bandwidth of the mixer:

$$BW = 2p_0 \frac{1}{2\pi RC} \tag{5.20}$$

With this extra addition the periodic transfer function is approximated as:

$$H_n(f_o) = \underbrace{e^{-j2\pi n f_s t_0}}_{\text{Time shift}} \underbrace{\frac{(1 - e^{-j2\pi\frac{1}{2}n})}{2}}_{\text{Balancing}} \underbrace{\text{sinc}(p_0 n) e^{-j2\pi\frac{p_0}{2}n}}_{\text{Harmonic Gain}} \underbrace{\frac{1}{1 + j\frac{f_o}{2p_0 f_{rc}}}}_{\text{Bandwidth}} \tag{5.21}$$

The relative magnitude error between equation 5.1 and equation 5.21 for several duty cycles and bandwidths is shown in table 5.2. A relative magnitude error less then 0.5% is achieved for $f_{rc} < \frac{f_s}{8}$. In this case the relative phase error is less then 5 degrees.

Table 5.2: Maximum magnitude approximation error for $f_o < f_s$ (1^{st}, 3^{nd} and 5^{nd} harmonic)

	$f_{rc} = \frac{f_s}{2}$	$f_{rc} = \frac{f_s}{4}$	$f_{rc} = \frac{f_s}{8}$
$p_0 = \frac{1}{2}$	0%	0%	0%
$p_0 = \frac{1}{3}$	5%	1.5%	0.5%
$p_0 = \frac{1}{4}$	5%	1.5%	0.5%
$p_0 = \frac{1}{6}$	7%	2%	0.5%
$p_0 = \frac{1}{8}$	1%	0.2%	0.05%

Unfortunately the addition of the bandwidth term has not been derived from the original expressions, due to mathematical difficulties.

5.3 Summary

In this section the periodic transfer function of the double balanced frequency converter model has been examined and transformed. It was proved that when the cutoff frequency of the RC network is swept to infinity the resulting expressions are equal to the expressions derived earlier for the double balanced sampling mixer. Also it shown that a duty cycle of 50 % transforms the expressions into the double balanced switching mixer expressions. The expressions for the Tayloe mixer are retrieved by setting a duty cycle of 25%.

Furthermore an approximate simplified expression for the conversion gain, noise figure and bandwidth was derived, only valid when the bandwidth of the mixer is smaller then 10 % of the RF frequency (narrowband). It was concluded that in the narrowband situation a duty cycle of 25 % gives the best balance between conversion loss and noise figure.

Chapter 6

RF Frontend Design

In the previous chapter is has been proved that the Tayloe mixer with 25 % duty cycle provides the best balance between noise figure and conversion loss. In this chapter a RF front end is designed using this mixer in standard 65 nm CMOS technology with a maximum gate-channel voltage of 1.2 V.

6.1 Top Level Design

A sample front end receiver is designed and simulated. The channel is chosen at 1 GHz with 20 MHz bandwidth. Image rejection is done with quadrature mixing. A double balanced architecture was chosen because of low conversion loss and robustness against second order distortion effects (described by Razavi [10]).

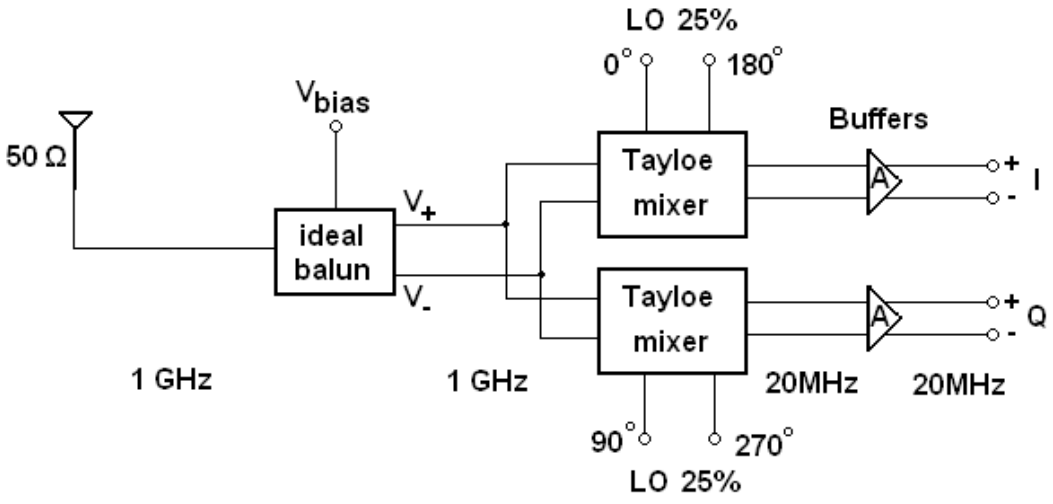

Figure 6.1: Receiver Design

Figure 6.1 gives an overview of the example receiver. The ideal balun transform the single ended antenna into a double balanced one. The second function of the balun is to provide a DC bias voltage for the mixer and buffers. The Tayloe mixer down converts the signal into an in-phase and quadrature signal at baseband. The buffers provide two times voltage gain to loosen the noise figure requirements of the preceding stages and to convert the moderate

output impedance of the mixer into a low output impedance. The target noise figure of the entire receiver is 5.0dB and the linearity should be designed as high as possible.

6.2 Circuit Level Design

6.2.1 Antenna

For a double balanced mixer to operate the voltage coming from the antenna should be balanced as well. An ideal balun transforms the single ended voltage into a double balanced voltage. The common mode of the output balanced voltage is set to a bias voltage required for the buffer.

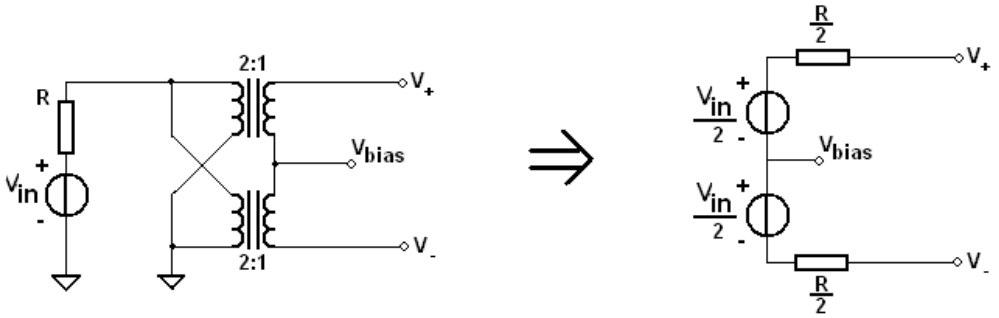

Figure 6.2: Balanced antenna model

In essence the receiver is sensing the voltage on the antenna. Typical receivers with LNA's first divide the voltage in half by impedance matching. The input signal power is defined in dBm, as the power dissipated in the 50 Ohm resistor when matching impedances. So at a defined input power, the input voltage at the input port of the receiver (after the antenna) is twice as high for a voltage sensing receiver.

The result is two times voltage gain with respect to the impedance matched case. The downside is the reduction of the IPx numbers with 6dB, since the input voltage is twice as high. The trade off is made between voltage gain and linearity.

6.2.2 Clock Driver

The mixer requires a clock signal to drive the switches. The focus in this project is not on clock generation, so it is assumed that the required clock signals are available with correct duty cycle and phase. It is further assumed that the clock signals are pure block waves switching between the negative and positive supply rail. In reality no clock generating circuit has these properties, so an inverter buffer is added to add realistic rise and fall times to the block wave and to provide a realistic output impedance.

In general, the linearity of a switch becomes better when the driving signal becomes larger in magnitude. Because of supply rail limitations, the maximum clock amplitude available is $1.2V$. For design reasons the channel voltage of the switches might be higher then the negative supply rail, so in order to reach maximum channel-gate voltage the clock has to be raised in voltage level as well.

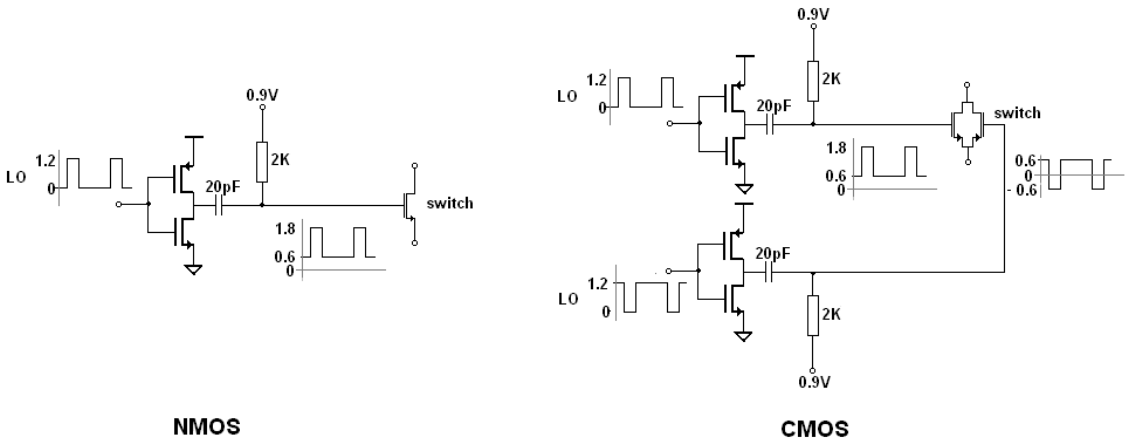

Figure 6.3: Clock bias circuit

The circuit used for raising the clock signals is shown in figure 6.3. The inverters are used to simulate realistic rise and fall times.

6.2.3 Mixer

The main design point for the mixer is the implementation of the switches. A MOSFET is ideal for switching purposes. Figure 6.4 shows the two mostly used implementations.

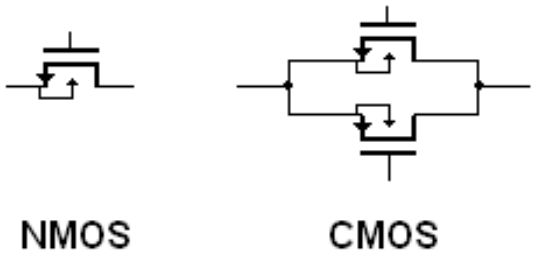

Figure 6.4: Transistor switches

In the NMOS implementation, the channel has a certain voltage level. When the gate voltage is equal to the channel voltage, the source drain resistance is very big and hence the transistor is off. When the gate voltage is well above the channel voltage (with a maximum of $1.2V$ for the 65 nm process) the source drain voltage is very low and the transistor is on. The transistor then operates in the linear region, since the gate source voltage minus the threshold voltage is much higher then the source drain voltage.

For achieving 20 MHz of bandwidth, the capacitor value is calculated using equation 5.20:

$$C = \frac{1}{2}\frac{1}{2\pi \cdot 50\Omega \cdot 20MHz} = 80pF \tag{6.1}$$

However, the input resistance seen by the mixer is not 50Ω but 25Ω because of the transformer (figure 2.14). Therefore the capacitance to ground is two times C, or 160 pF.

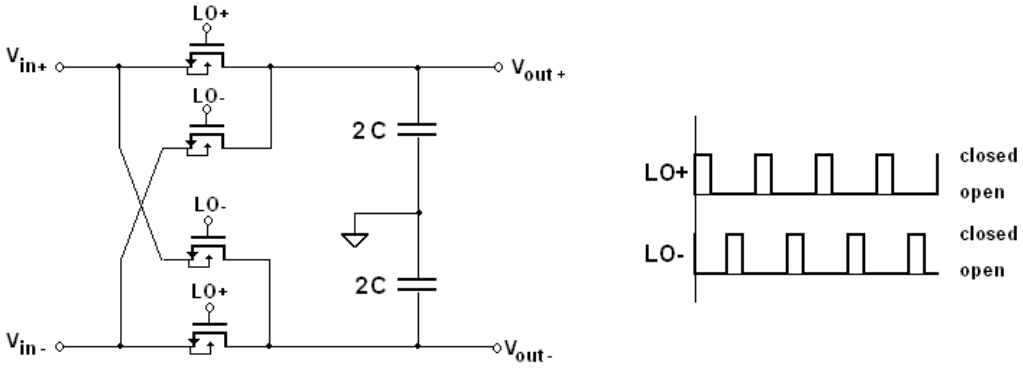

Figure 6.5: NMOS Tayloe mixer

For the CMOS implementation, a PMOS transistor is placed parallel to the NMOS transistor, thus forming transmission gates. When the MOSFET's are on, the resistance is lower because of the parallel configuration. The width of both NMOS and PMOS is chosen equal to equalize the gate capacitance.

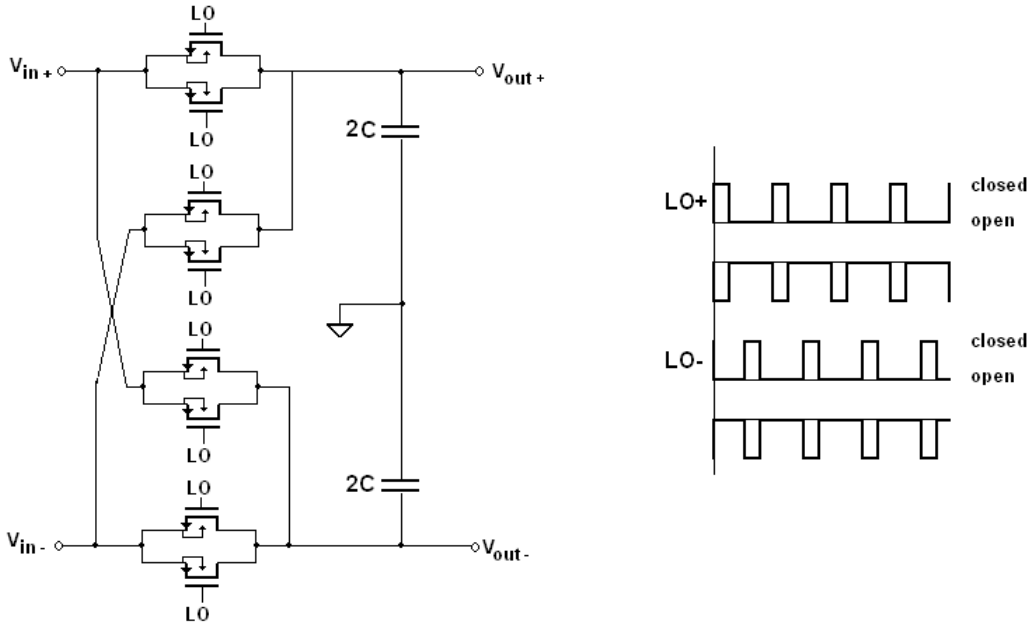

Figure 6.6: CMOS Tayloe mixer

For IQ image rejection, a duplicate mixer is added with all clock periods shifted a quarter time the sample time. The inputs of both mixers are connected together. The linearity is optimized by applying as high a channel gate voltage swing as possible. The noise is minimized to acceptable levels by scaling the width of the transistors.

6.2.4 Buffer

In the analysis of the mixer it was assumed that the block following it has a high input impedance. Also, a bit more gain in the receiver helps to decrease the influence of back

end receiver blocks on the noise figure. Therefore a buffer is being implemented following the mixer, having two times voltage gain and a high linearity. The inverter has been reported by Nauta [8] to have good linearity properties, so this is used as a base design.

The inverter ideally has zero second order distortion and reduced third order distortion. Because of the low supply voltage of 1.2V, only 0.6 V is available per transconductor. Klumperink and Nauta have shown that for low voltage headrooms the MOSFET in strong inversion provides the highest linearity [9]. For higher supply voltages the degenerated MOSFET in strong inversion gives higher performance. Klumperink and Nauta also derive that transconductor design should concentrate on linearity properties, whereas the noise can be optimized by admittance scaling.

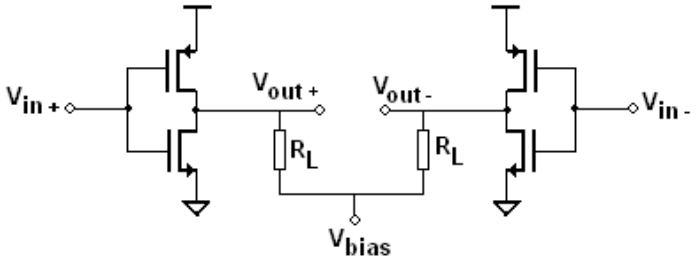

Figure 6.7: Inverter

The inverter schematic is shown in figure 6.7. The PMOS has lower mobility, so its width is scaled to 3.2 times the width of the NMOS to ensure that both transistors have the same g_m. The length of PMOS and NMOS is kept at $0.5\mu m$ which improves linearity with respect to minimum length transistors. Both the transistors are biased at half the supply rail at 600 mV, ensuring that the gate-source voltage of both transistors is equal.

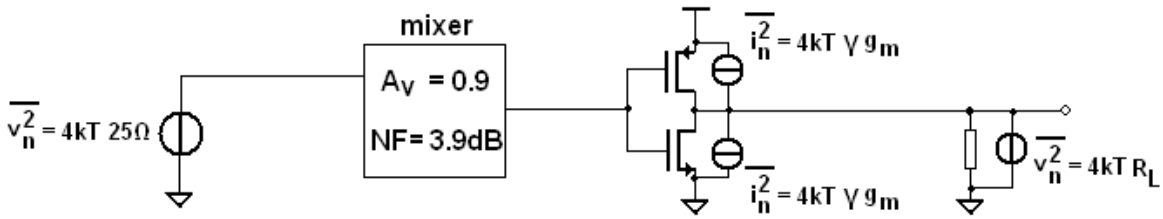

Figure 6.8: Circuit half noise model

To achieve two times voltage gain, $A_v = R \cdot g_m = 2$. To determine the receiver noise figure, the noise is analyzed from the antenna through one-half of the mixer and one buffer. Figure 6.8 shows the noise contributions from every part of the circuit, only including thermal noise. Because this analysis is focused on one circuit half of the double balanced structure, the antenna impedance is the half of 50Ω. Another way of looking at it is that the balun transforms the antenna impedance to 25Ω. The output referred contribution of each noise source is calculated:

$$\bar{v^2}_{n,antenna} = 4kT25\Omega \cdot 0.9^2 \cdot 10^{\frac{3.9}{10}} \cdot 2^2 g_m^2 R_L^2 \tag{6.2}$$
$$\bar{v^2}_{n,NMOS} = 4kT\gamma g_m R_L^2 \tag{6.3}$$
$$\bar{v^2}_{n,PMOS} = 4kT\gamma g_m R_L^2 \tag{6.4}$$
$$\bar{v^2}_{n,R_L} = 4kTR_L \tag{6.5}$$

Where k is the Boltzmann constant and T is the temperature in Kelvin. According to Leung the noise figure can now be calculated by [7]:

$$NF = 10 \cdot \log\left(\frac{N_{output} + N_{internal}}{G \cdot N_{input}}\right) \tag{6.6}$$

Where $N_{internal}$ is the output referred noise power of the noise sources inside the circuit, N_{output} is the output referred noise power of the input noise source, N_{input} is the input referred noise power of the input noise source and G is the total power gain. Filling in the noise powers:

$$NF = 10 \cdot \log\left(\frac{\bar{v^2}_{n,antenna} + \bar{v^2}_{n,NMOS} + \bar{v^2}_{n,PMOS} + \bar{v^2}_{n,R_L}}{4kT25\Omega \cdot 0.9^2 \cdot (2g_m R_L)^2}\right) \tag{6.7}$$
$$= 10 \cdot \log\left(\frac{25\Omega \cdot 0.9^2 \cdot 10^{\frac{3.9}{10}} \cdot (2g_m R_L)^2 + 2 \cdot \gamma g_m R_L^2 + R_L}{25\Omega \cdot 0.9^2 \cdot (2g_m R_L)^2}\right) \tag{6.8}$$
$$= 10 \cdot \log\left(10^{\frac{3.9}{10}} + \frac{\frac{1}{2}\frac{1}{g_m}\gamma + \frac{R}{(2g_m R)^2}}{25\Omega \cdot 0.9^2}\right) \tag{6.9}$$
$$= 10 \cdot \log\left(10^{\frac{3.9}{10}} + \frac{\frac{1}{2g_m}(\gamma + \frac{1}{A_v})}{25\Omega \cdot 0.9^2}\right) \tag{6.10}$$

From this equation it can be concluded the noise contribution of the load resistor with respect to the noise contribution of the transistors is determined by the voltage gain A_v and γ. In this case $A_v = 2$ and $\gamma = \frac{2}{3}$, so the transistors contribute slightly more to the noise then the resistor does. Evaluating this equation for $g_m = 100mS$ results in a total receiver front end Noise Figure of 4.4 dB. This leaves some room for flicker noise and a dropping mixer gain for high frequency until the Noise Figure of 5.0 dB is reached. For the NMOS a width of $1000\mu m$ is needed and for the PMOS a width of $3200\mu m$ is needed to get $g_m = 100mS$. To get the two times voltage gain the load resistor R_L is 10Ω.

6.3 Block Simulation Results

Simulated performance of the individual front end blocks.

6.3.1 Clock Driver

The time response of the CMOS clock driver is shown in figure 6.9. The clock driver ensures a common channel voltage for both NMOS and PMOS, while maintaining the full supply voltage swing over each gate.

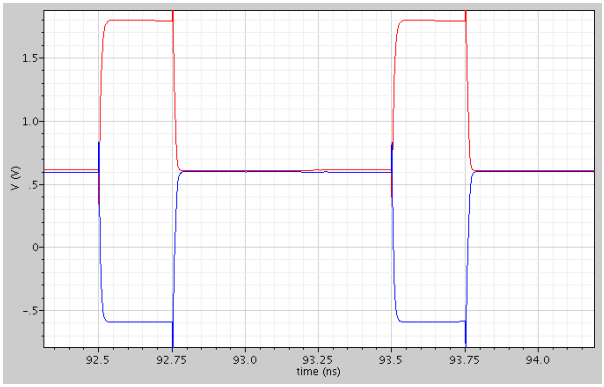

Figure 6.9: Clock bias circuit time response

6.3.2 Mixer

The periodic transfer function of the NMOS mixer is shown in figure 6.10, with respect to output frequency and with respect to input frequency. The simulation verifies that the mixer has a conversion loss of 0.9dB since the gain of the first harmonic around DC baseband is 0.9 . Furthermore the bandwidth is lower then 20 MHz, caused by the extra switch resistance of the MOSFET transistors. The simulation shows this extra resistance to be 5Ω per transistor, so equation 6.1 has to be modified:

$$C = \frac{1}{2}\frac{1}{2\pi \cdot (50+10)\Omega \cdot 20MHz} = 65pF \tag{6.11}$$

Double balancing then requires the output node capacitance to be 130pF to ground. The CMOS mixer has exactly the same transfer function, which is therefore not shown.

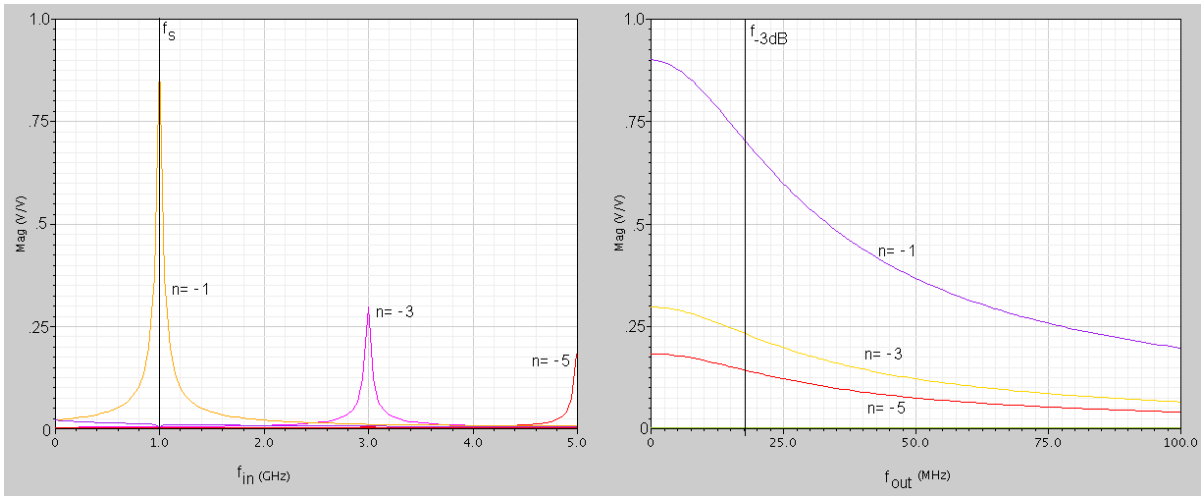

Figure 6.10: NMOS Conversion Gain

To optimize the Noise Figure simulations were performed with different transistor lengths. Figure 6.11 shows the resulting noise figure for both CMOS and NMOS mixer. It appears that the CMOS mixer achieves the same noise figure as the NMOS mixer at half the transistor width. Such is to be expected since a PMOS and NMOS in parallel have effectively twice the width of a single NMOS transistor. Therefore, the transistor width for NMOS is chosen to be

200μm and the width for CMOS is chosen to be 100μm. The mixer noise figure then becomes 4.1 dB.

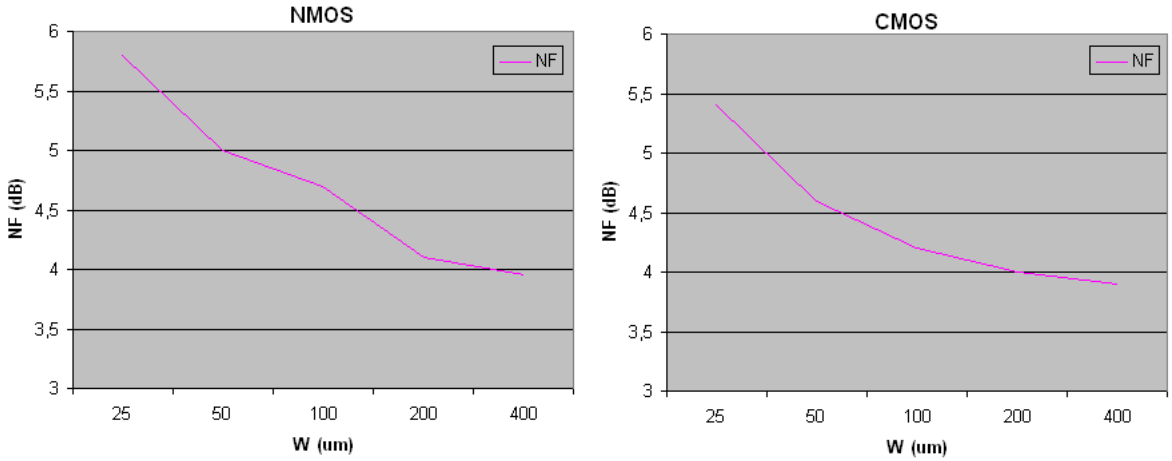

Figure 6.11: Mixer Noise Figure vs transistor Width

To verify the statement that the mixer IIP3 drops for lower gate LO drive, IIP3 simulations were performed with several LO drives. Figure 6.12 shows indeed a descending IIP3 for decreasing LO drive.

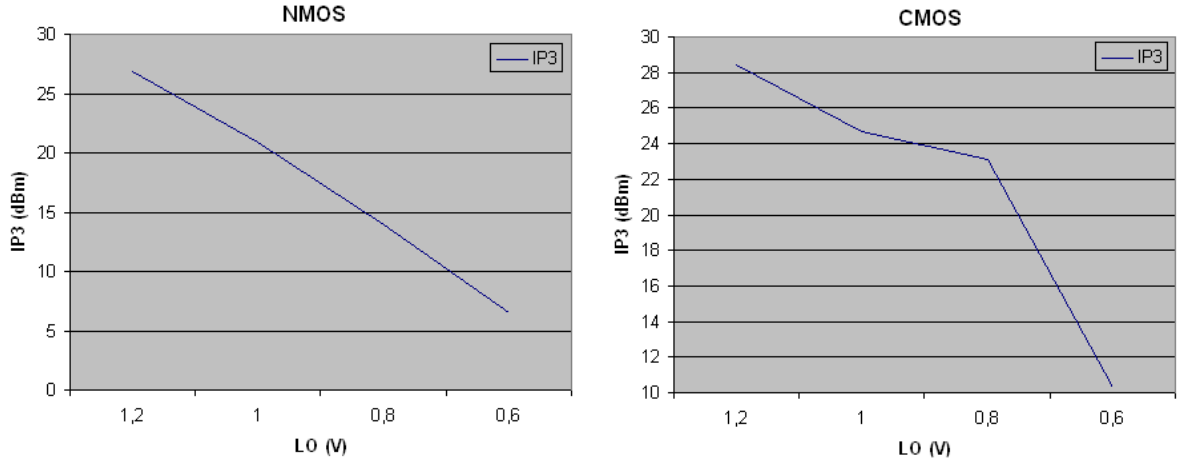

Figure 6.12: Mixer IIP3 vs LO Drive

6.3.3 Buffer

The voltage amplification for the buffer is shown in figure 6.13. In the whole bandwidth the voltage amplification is greater then two, as desired.

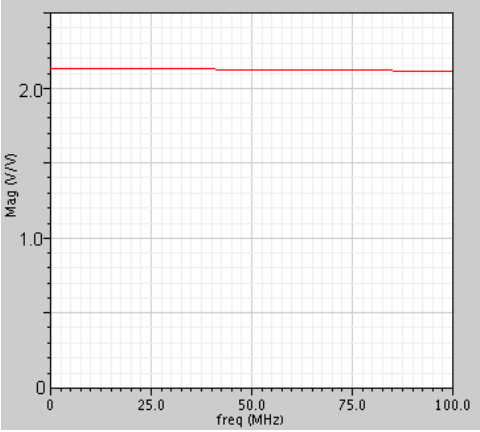

Figure 6.13: Buffer voltage amplification

The IIP3 of the buffer is shown in figure 6.14. The IIP3 is +12dBm and the -1dB compression point is at -8 dBm. The low supply voltage limits the options to further improve the non-linearity.

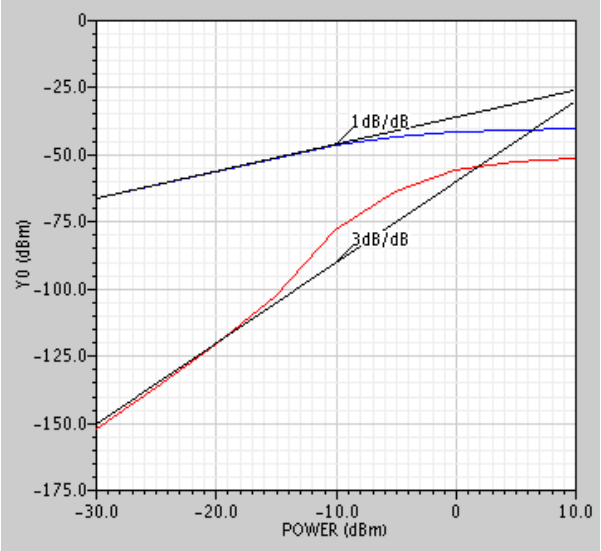

Figure 6.14: Buffer IIP3

The output impedance of the buffer is 10Ω, suitable for voltage driving the next stage in the amplifier. The gate-source capacitance of the PMOS is 11pF and the gate-source capacitance of the NMOS is 4pF. The combined 15pF of buffer input capacitance has to be subtracted from the 130pF calculated in equation 6.11 to get the correct bandwidth.

6.4 Receiver Simulation Results

Putting together the designed blocks a total receiver front end is created. Figure 6.15 shows the NMOS front end with all device dimensions. The CMOS receiver is similar. The conversion gain versus output frequency is shown in figure 6.16. The voltage amplification is 3.5 which is equal to 10.5 dB.

The noise figure versus output frequency is shown in figure 6.17. In baseband from 1 MHz to 18 MHz the noise figure is below 5.0 dB. Below 1 MHz the flicker noise from the buffer MOSFET's is raising the noise figure above 5 dB.

The IIP3 versus output frequency is shown in figure 6.18. The resulting IIP3 is higher then +12dBm and the -1dB compression point is -5 dBm.

DC supply power simulations were performed. The resulting power figures are shown in table 6.1.

Table 6.1: DC Power Dissipation

	Clock Driver	Mixer	Buffer	Total
NMOS	$4 \cdot 2$ mW	0 mW	$4 \cdot 11$ mW	52 mW
CMOS	$8 \cdot 2$ mW	0 mW	$4 \cdot 11$ mW	60 mW

The balancing of the receiver cancels out antenna radiation. In the presence of mismatch, the circuit will become unbalanced and LO signals can leak through to the antenna. For the NMOS receiver the antenna voltage resulting from the LO signals have been measured while mismatching the width of a single switch resistor in the mixer. In Table 6.2 the mismatch results are shown in V.

Table 6.2: NMOS Receiver antenna radiation with a single mismatched transistor

f	0%	1%	5%
1 GHz	$< 100nV$	$85\mu V$	$430\mu V$
3 GHz	$< 100nV$	$14\mu V$	$76\mu V$
5 GHz	$< 100nV$	$30\mu V$	$151\mu V$

The antenna impedance is 50Ω. Table 6.3 shows the mismatch results in dBm. In a practical CMOS process the mismatch is below 1%, resulting in antenna radiation below -70dBm.

Table 6.3: NMOS Receiver antenna radiation with a single mismatched transistor

f	0%	1%	5%
1 GHz	$< -125dBm$	$-72dBm$	$-54dBm$
3 GHz	$< -125dBm$	$-84dBm$	$-70dBm$
5 GHz	$< -125dBm$	$-77dBm$	$-63dBm$

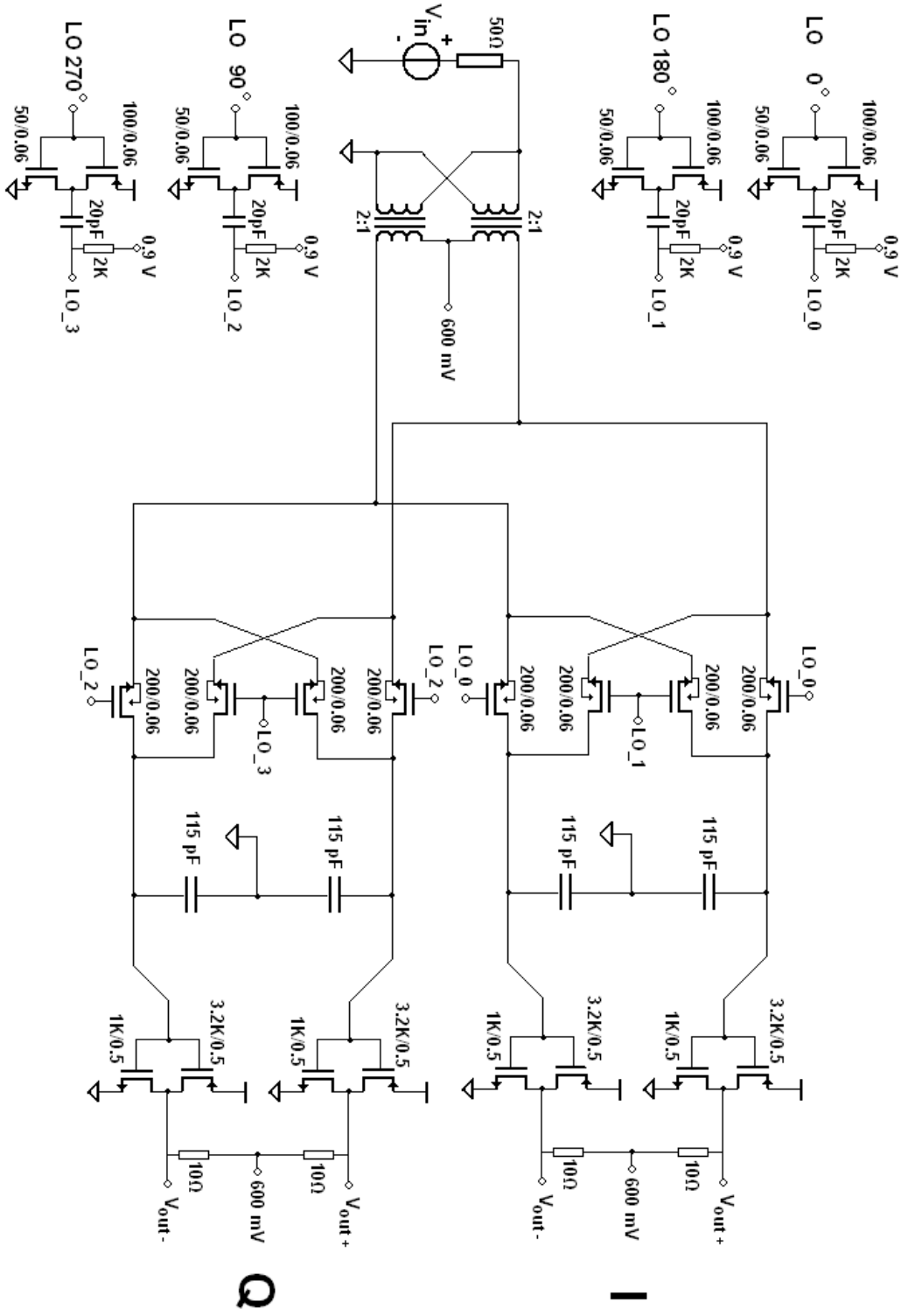

Figure 6.15: NMOS receiver frontend

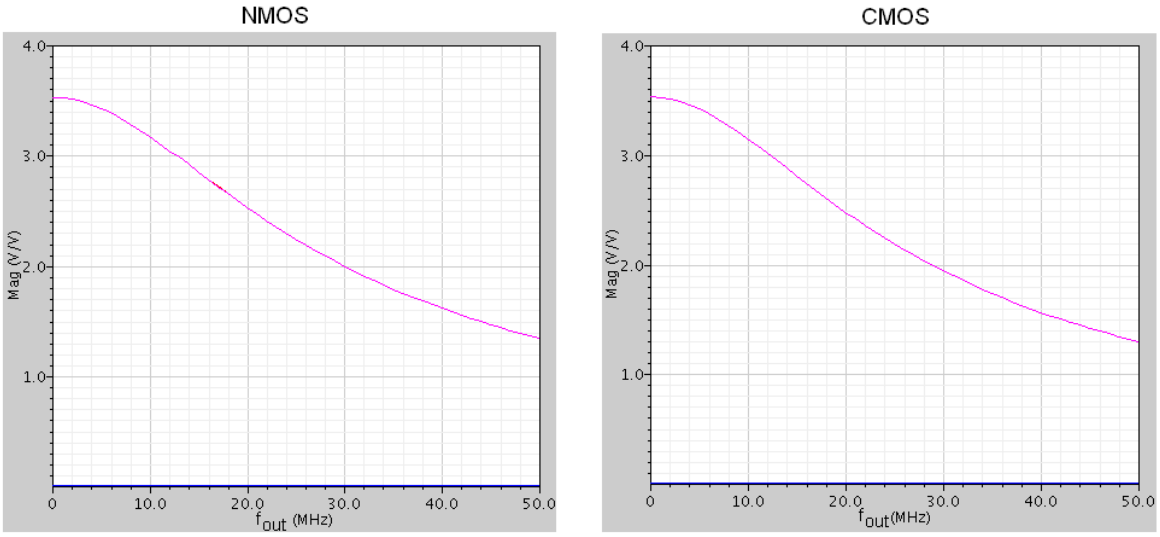

Figure 6.16: Front end voltage gain

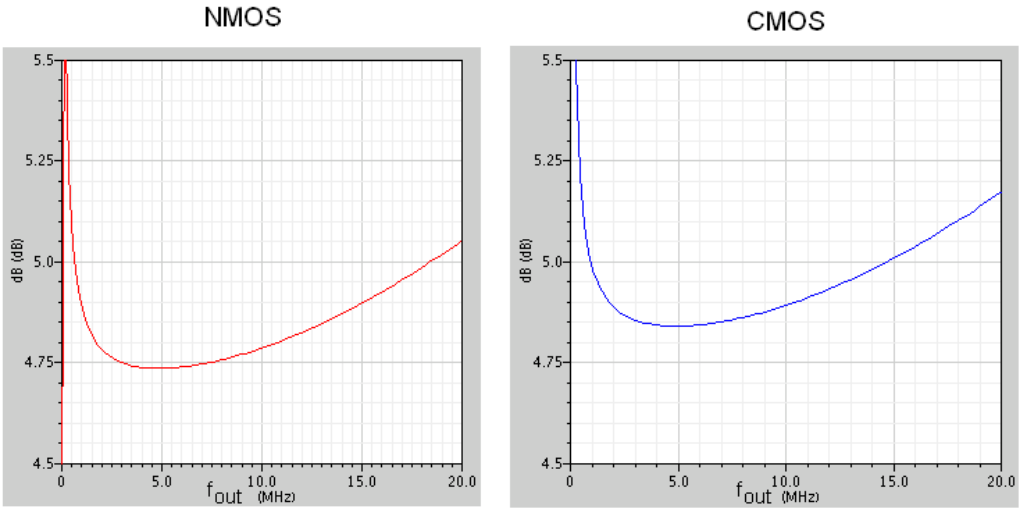

Figure 6.17: Front end Noise Figure

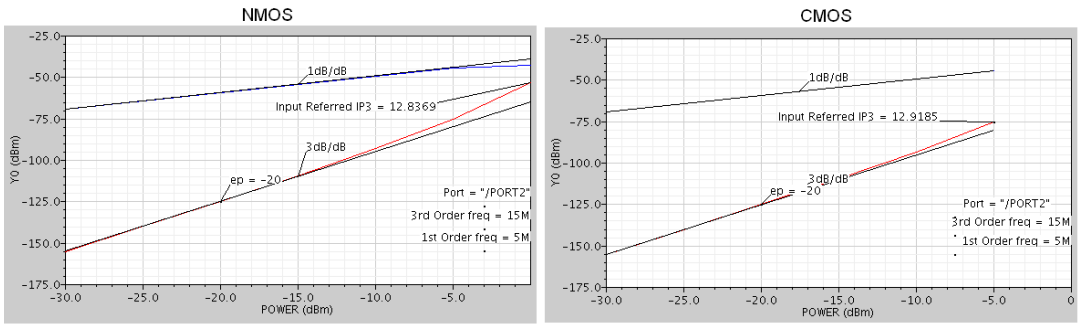

Figure 6.18: Frontend IIP3

6.5 Summary

A receiver front end using the Tayloe mixer was designed for a RF frequency of 1GHz and with a bandwidth of 20 MHz. A conversion gain of 10.5 dB was achieved, with a noise figure of less then 5.0 dB in the band of interest. The IIP3 is +12 dBm and the -1dB compression point is at -5 dBm. Both are limited by the voltage buffer following the mixer. Both in-phase and quadrature components are generated by having parallel mixer paths. Furthermore, the output impedance of the output buffers is 10Ω.

Chapter 7

Conclusions

A model has been presented to analyze the frequency domain behavior of the switching, sampling and Tayloe mixer. This frequency converter model has been analyzed using Linear Periodically Time Variant theory, resulting in closed form expressions for the periodic transfer function. With these expressions the conversion gain, bandwidth and Noise Figure of the single and double mixers can be calculated exactly.

Furthermore, an approximation of the found periodic transfer function has been formulated for narrowband channels, which directly translates the duty cycle parameter to conversion gain and Noise Figure, and the bandwidth parameter to the baseband bandwidth. It was concluded that a double balanced Tayloe mixer with 25% duty cycle provides the best balance between noise figure (3.9dB) and conversion loss(0.9dB).

An example RF receiver front end was designed and simulated in 65 nm CMOS technology. The channel was chosen at 1 GHz with 20 MHz bandwidth. A conversion gain of 10.5 dB was achieved with a noise figure of 5.0 dB. The IIP3 of +12 dBm and -1dB compression point of -5 dBm are limited by the low supply voltage of the output buffers. It can therefore be concluded that a receiver front end with high linearity and moderate noise figure can be implemented using the Tayloe mixer.

Chapter 8

Recommendations

In this Master thesis the linearity of the Tayloe mixer was not calculated, but assumed to be high enough due to the passive nature of the mixer. In future work a Volterra series representation of Tayloe mixer might help to calculate the distortion. From a design point of view such a representation might not be necessary since it is easy to design highly linear switch MOSFET's. But from a theoretical point of view it is satisfying to have the complete picture.

The linearity of the simulated front end was limited by the voltage buffers following the mixer. A commonly known trick to improve linearity is to use emitter degeneration, but the supply voltage proved to be too low to take advantage of this trick. It is questionable whether a supply voltage of 1.2V allows for IIP3 numbers much higher then +10dBm for non-feedback g_m stages. It might be necessary to put more research into highly linear IF amplifiers with low supply voltages. Also, a feedback amplifier might be one of the options to achieve higher linearity.

Appendix A

Identities

In this appendix, some useful mathematical identities are given to assist the reader.

Euler

$$e^{jx} = \cos(x) + j\sin(x) \tag{A.1}$$
$$e^{-jx} = \cos(x) - j\sin(x) \tag{A.2}$$

$$\cos(x) = \frac{e^{jx} + e{-}jx}{2} \tag{A.3}$$
$$\sin(x) = \frac{e^{jx} - e{-}jx}{j2} \tag{A.4}$$

$$sinc(x) = \frac{\sin(\pi x)}{\pi x} = \frac{e^{j\pi x} - e^{-j\pi x}}{j2\pi x} \tag{A.5}$$

$$cosh(x) = \cos(jx) = \frac{e^{x} + e^{-x}}{2} jsinh(x) = \sin(jx) = \frac{e^{x} - e^{-x}}{2j} \tag{A.6}$$

Complex numbers

$$|z| = \sqrt{x^2 + y^2} \tag{A.7}$$
$$\phi = arg(x, y) \tag{A.8}$$

$$z = x + jy = |z|\,(\cos(\phi) + j\sin(\phi)) = |z|\,e^{j\phi} \tag{A.9}$$
$$z = x - jy = |z|\,(\cos(\phi) - j\sin(\phi)) = |z|\,e^{-j\phi} \tag{A.10}$$

$$\frac{1}{x + jy} = \frac{x - jy}{x^2 + y^2} \tag{A.11}$$
$$\frac{1}{z} = \frac{z^*}{|z|^2} \tag{A.12}$$

Dirac pulse

$$x(t)\delta(t-t_0) = x(t_0)\delta(t-t_0) \tag{A.13}$$

$$x(t) * \delta(t-t_0) = x(t-t_0) \tag{A.14}$$

A periodic Dirac pulse (the Dirac comb) can be represented by a Fourier series. The period time is T_s, the period frequency is $F_s = \frac{1}{T_s}$ and the period angular frequency is $\omega_s = 2\pi F_s$.

$$x(t) = \sum_{n=-\infty}^{\infty} \delta(t - nT_s) = \frac{1}{T_s} \sum_{n=-\infty}^{\infty} e^{j2\pi nt\frac{1}{T_s}} \tag{A.15}$$

$$X(f) = F_s \sum_{n=-\infty}^{\infty} \delta(f - nF_s) = \sum_{n=-\infty}^{\infty} e^{-j2\pi fnT_s} \tag{A.16}$$

Appendix B

Derivations

B.1 Laplace

In this section the time response of a first order RC filter is derived. Assuming a sinusoid input, the input/output conditions are defined as:

$$V_{in}(t) = e^{j2\pi f_i(t+t_p)} = e^{j2\pi f_i t_p} e^{j2\pi f_i t} \tag{B.1}$$

$$V_{out}(0^-) = v(0^-) \tag{B.2}$$

Transforming $V_{in}(t)$ to the Laplace domain:

$$V_{in}(s) = \frac{e^{j2\pi f_i t_p}}{s - j2\pi f_i} \tag{B.3}$$

The differential equation of the circuit is:

$$RC\frac{dV_{out}(t)}{dt} + V_{out}(t) = V_{in}(t) \tag{B.4}$$

Transforming to the Laplace domain:

$$V_{out}(s)(sRC + 1) = V_{in}(s) + RCv(0^-) \tag{B.5}$$

$$V_{out}(s) = \frac{V_{in}(s)}{sRC + 1} + \frac{RCv(0^-)}{sRC + 1} \tag{B.6}$$

Inserting the Laplace expression for $V_{in}(s)$:

$$V_{out}(s) = \frac{e^{j2\pi f_i t_p}}{(s - j2\pi f_i)(sRC + 1)} + \frac{RCv(0^-)}{sRC + 1} \tag{B.7}$$

Define $RC = \frac{1}{2\pi f_{rc}}$:

$$V_{out}(s) = \frac{e^{j2\pi f_i t_p} \cdot 2\pi f_{rc}}{(s - j2\pi f_i)(s + 2\pi f_{rc})} + \frac{v(0^-)}{s + 2\pi f_{rc}} \tag{B.8}$$

Performing partial fraction expansion:

$$V_{out}(s) = \frac{1}{1 + j\frac{f_i}{f_{rc}}} \frac{e^{j2\pi f_i t_p}}{s - j2\pi f_i} - \frac{1}{1 + j\frac{f_i}{f_{rc}}} \frac{e^{j2\pi f_i t_p}}{s + 2\pi f_{rc}} + \frac{v(0^-)}{s + 2\pi f_{rc}} \tag{B.9}$$

Transforming back to the time domain:

$$V_{out}(t) = \frac{1}{1+j\frac{f_i}{f_{rc}}} e^{j2\pi f_i t_p} e^{j2\pi f_i t} - \frac{1}{1+j\frac{f_i}{f_{rc}}} e^{j2\pi f_i t_p} e^{-2\pi f_{rc} t} + v(0^-) e^{-2\pi f_{rc} t} \tag{B.10}$$

Or in different form:

$$V_{out}(t) - v(0^-) e^{-2\pi f_{rc} t} = \frac{e^{j2\pi f_i t} - e^{-2\pi f_{rc} t}}{1+j\frac{f_i}{f_{rc}}} e^{j2\pi f_i t_p} \tag{B.11}$$

B.2 Single Balanced Difference Equation

The differential equations for the single balanced Tayloe mixer are given by:

$$\begin{cases} RC\frac{dV_{out}(t)}{dt} + V_{out}(t) = V_{in}(t) & , t_0 + nT_s < t < t1 + nT_s \\ V_{out}(t) = V_{out}(nT_s + t_1) & , t_1 + nT_s < t < t0 + (n+1)T_s \end{cases} \tag{B.12}$$

Assuming a sinusoid input:

$$V_{in}(t) = e^{j\omega_i t} \tag{B.13}$$

For phase 0 equation B.11 is used to calculate the final value at $nT_s + t_1$, therefore $t = p_0 T_s$ and $t_p = nT_s + t_0$:

$$V_{out}(nT_s + t_1) - e^{-2\pi f_{rc} p_0 T_s} V_{out}(nT_s + t_0) = \frac{e^{j2\pi f_i p_0 T_s} - e^{-2\pi f_{rc} p_0 T_s}}{1+j\frac{f_i}{f_{rc}}} e^{j2\pi f_i (nT_s + t_0)} \tag{B.14}$$

For phase 1 the difference equation is trivial:

$$V_{out}((n+1)T_s + t_0) = V_{out}(nT_s + t_1) \tag{B.15}$$

Combining the two difference equations:

$$V_{out}((n+1)T_s + t_0) - e^{-2\pi f_{rc} p_0 T_s} V_{out}(nT_s + t_0) = \frac{e^{j2\pi f_i p_0 T_s} - e^{-2\pi f_{rc} p_0 T_s}}{1+j\frac{f_i}{f_{rc}}} e^{j2\pi f_i nT_s} e^{j2\pi f_i t_0} \tag{B.16}$$

By using the substitution $E_n = V_{out}(nT_s + t1)$ this equation can be solved using the Z-transform:

$$zE_n(z) - e^{-2\pi f_{rc} p_0 T_s} E_n(z) = \underbrace{\frac{e^{j2\pi f_i p_0 T_s} - e^{-2\pi f_{rc} p_0 T_s}}{1+j\frac{f_i}{f_{rc}}}}_{C_1(f_i)} \underbrace{\frac{z}{z - e^{j2\pi f_i T_s}}}_{\text{input sinusoid}} e^{j2\pi f_i t_0} \tag{B.17}$$

$$E_n(z) = C_1(f_i) \frac{z}{(z - e^{-2\pi f_{rc} p_0 T_s})(z - e^{j2\pi f_i T_s})} e^{j2\pi f_i t_0} \tag{B.18}$$

Doing partial fraction expansion:

$$E_n(z) = C_1(f_i) \left[\underbrace{\frac{1}{e^{j2\pi f_i T_s} - e^{-2\pi f_{rc} p_0 T_s}} \frac{z}{z - e^{j2\pi f_i T_s}}}_{\text{steady state}} + \underbrace{\frac{1}{e^{-2\pi f_{rc} p_0 T_s} - e^{j2\pi f_i T_s}} \frac{1}{z - e^{-2\pi f_{rc} p_0 T_s}}}_{\text{initial value}} \right] e^{j2\pi f_i t_0} \tag{B.19}$$

When we are applying this in the frequency domain, the initial value response is not important. When doing a frequency domain approach we assume that the sinusoids making up the input signal have been on the input of the circuit for all time. We are not interested in startup phenomenon. Therefore, the value of E_n in the time domain at the t_0 time instants is given by:

$$E_n = V_{out}(nT_s + t_0) = \frac{e^{j2\pi f_i p_0 T_s} - e^{-2\pi f_{rc} p_0 T_s}}{e^{j2\pi f_i T_s} - e^{-2\pi f_{rc} p_0 T_s}} \frac{1}{1 + j\frac{f_i}{f_{rc}}} e^{j2\pi f_i n T_s} e^{j2\pi f_i t_0} \tag{B.20}$$

Since the input is defined as $V_{in}(t) = e^{j2\pi f_i t}$, we can define a sort of transfer function relating the value of V_{out} at the instant t_0 to the input sinusoid. This transfer function is defined as G_0 in the following way:

$$V_{out}(nT_s + t_0) = G_0(f_i) e^{j2\pi f_i n T_s} \tag{B.21}$$

$$G(f_i) = \frac{e^{j2\pi f_i p_0 T_s} - e^{-2\pi f_{rc} p_0 T_s}}{e^{j2\pi f_i T_s} - e^{-2\pi f_{rc} p_0 T_s}} \frac{1}{1 + j\frac{f_i}{f_{rc}}} \tag{B.22}$$

$$G_0(f_i) = G(f_i) e^{j2\pi f_i t_0} \tag{B.23}$$

Then from equation B.14 the expression for the other switching instants is reconstructed:

$$V_{out}((n+1)T_s + t_0) = V_{out}(nT_s + t_0) e^{j2\pi f_i T_s} \tag{B.24}$$

$$= G_0(f_i) e^{j2\pi f_i T_s} e^{j2\pi f_i n T_s} \tag{B.25}$$

$$= G(f_i) e^{j2\pi f_i t_2} e^{j2\pi f_i n T_s} \tag{B.26}$$

$$V_{out}(nT_s + t_1) = V_{out}((n+1)T_s + t_0) \tag{B.27}$$

$$= G(f_i) e^{j2\pi f_i t_2} e^{j2\pi f_i n T_s} \tag{B.28}$$

In summary:

$$V_{out}(nT_s + t_k) = G_k(f_i) e^{j2\pi f_i n T_s} \tag{B.29}$$

$$G(f_i) = \frac{e^{j2\pi f_i h T_s} - e^{-2\pi f_{rc} h T_s}}{e^{j2\pi f_i T_s} - e^{-2\pi f_{rc} h T_s}} \frac{1}{1 + j\frac{f_i}{f_{rc}}} \tag{B.30}$$

$$G_0(f_i) = G(f_i) e^{j2\pi f_i t_0} \tag{B.31}$$

$$G_1(f_i) = G(f_i) e^{j2\pi f_i t_2} \tag{B.32}$$

$$G_2(f_i) = G(f_i) e^{j2\pi f_i t_2} \tag{B.33}$$

Figure B.1: Tayloe Mixer Single Balanced G_k

B.3 Double Balanced Difference equation

The differential equations for the double balanced Tayloe mixer are given by:

$$\begin{cases} RC\frac{dV_{out}(t)}{dt} + V_{out}(t) = V_{in}(t) & , t_0 + nT_s < t < t1 + nT_s \\ V_{out}(t) = V_{out}(nT_s + t_1) & , t_1 + nT_s < t < t2 + nT_s \\ RC\frac{dV_{out}(t)}{dt} + V_{out}(t) = -V_{in}(t) & , t_2 + nT_s < t < t3 + nT_s \\ V_{out}(t) = V_{out}(nT_s + t_3) & , t_3 + nT_s < t < t0 + (n+1)T_s \end{cases} \tag{B.34}$$

Assuming a sinusoid input:

$$V_{in}(t) = e^{j\omega_i t} \tag{B.35}$$

paragraph For phase 0 equation B.11 is used to calculate the final value at $nT_s + t_1$, therefore $t = p_0 T_s$ and $t_p = nT_s + t_0$:

$$V_{out}(nT_s + t_1) - e^{-2\pi f_{rc} p_0 T_s} V_{out}(nT_s + t_0) = \frac{e^{j2\pi f_i p_0 T_s} - e^{-2\pi f_{rc} p_0 T_s}}{1 + j\frac{f_i}{f_{rc}}} e^{j2\pi f_i (nT_s + t_0)} \tag{B.36}$$

For phase 1 the difference equation is trivial:

$$V_{out}(nT_s + t_2) = V_{out}(nT_s + t_1) \tag{B.37}$$

paragraph For phase 2 equation B.11 is used to calculate the final value at $nT_s + t_3$, therefore $t = p_2 T_s$ and $t_p = nT_s + t_2$:

$$V_{out}(nT_s + t_3) - e^{-2\pi f_{rc} p_2 T_s} V_{out}(nT_s + t_2) = -\frac{e^{j2\pi f_i p_2 T_s} - e^{-2\pi f_{rc} p_2 T_s}}{1 + j\frac{f_i}{f_{rc}}} e^{j2\pi f_i (nT_s + t_2)} \tag{B.38}$$

For phase 3 the difference equation is trivial:

$$V_{out}((n+1)T_s + t_0) = V_{out}(nT_s + t_3) \tag{B.39}$$

Combining the four latter equations reduces the order to two:

$$V_{out}(nT_s + t_1) = \frac{e^{j2\pi f_i p_0 T_s} - e^{-2\pi f_{rc} p_0 T_s}}{1 + j\frac{f_i}{f_{rc}}} e^{j2\pi f_i n T_s} e^{j2\pi f_i t_0} + e^{-2\pi f_{rc} p_0 T_s} V_{out}(nT_s + t_0) \tag{B.40}$$

$$V_{out}((n+1)T_s + t_0) - e^{-2\pi f_{rc} p_2 T_s} V_{out}(nT_s + t_1) = -\frac{e^{j2\pi f_i p_2 T_s} - e^{-2\pi f_{rc} p_2 T_s}}{1 + j\frac{f_i}{f_{rc}}} e^{j2\pi f_i n T_s} e^{j2\pi f_i t_2} \tag{B.41}$$

Substituting for $V_{out}(nT_s + t_1)$ yields a single difference equation:

$$\begin{aligned} V_{out}((n+1)T_s + t_0) - e^{-2\pi f_{rc}(p_0+p_2)T_s} V_{out}(nT_s + t_0) = \\ - \frac{e^{j2\pi f_i p_2 T_s} - e^{-2\pi f_{rc} p_2 T_s}}{1 + j\frac{f_i}{f_{rc}}} e^{j2\pi f_i (p_0+p_1) T_s} e^{j2\pi f_i (nT_s + t_0)} \\ + \frac{e^{j2\pi f_i p_0 T_s} - e^{-2\pi f_{rc} h_0 T_s}}{1 + j\frac{f_i}{f_{rc}}} e^{-2\pi f_{rc} p_2 T_s} e^{j2\pi f_i (nT_s + t_0)} \end{aligned} \tag{B.42}$$

$$\begin{aligned} &V_{out}((n+1)T_s + t_0) - e^{-2\pi f_{rc}(p_0+p_2)T_s} V_{out}(nT_s + t_0) = \\ &\frac{-(e^{j2\pi f_i p_2 T_s} - e^{-2\pi f_{rc} p_2 T_s}) e^{j2\pi f_i (p_0+p_1) T_s} + (e^{j2\pi f_i p_0 T_s} - e^{-2\pi f_{rc} p_0 T_s}) e^{-2\pi f_{rc} p_2 T_s}}{1 + j\frac{f_i}{f_{rc}}} e^{j2\pi f_i (nT_s + t_0)} \end{aligned} \tag{B.43}$$

Now we apply the restricting conditions for double balanced operation: $p_0 = p_2, p_1 = p_3, p_0 + p_1 = \frac{1}{2}, p_2 + p_3 = \frac{1}{2}$. The resulting difference equation becomes:

$$V_{out}((n+1)T_s + t_0) - e^{-2\pi f_{rc} 2p_0 T_s} V_{out}(nT_s + t_0) = \frac{(e^{j2\pi f_i p_0 T_s} - e^{-2\pi f_{rc} p_0 T_s})(-e^{j2\pi f_i \frac{1}{2} T_s} + e^{-2\pi f_{rc} p_0 T_s})}{1 + j\frac{f_i}{f_{rc}}} e^{j2\pi f_i n T_s} e^{j2\pi f_i t_0} \tag{B.44}$$

By using the substitution $E_n = V_{out}(nT_s + t1)$ this equation can be solved using the Z-transform:

$$zE_n(z) - e^{-2\pi f_{rc} 2hT_s} E_n(z) = \underbrace{\frac{(e^{j2\pi f_i p_0 T_s} - e^{-2\pi f_{rc} p_0 T_s})(-e^{j2\pi f_i \frac{1}{2} T_s} + e^{-2\pi f_{rc} p_0 T_s})}{1 + j\frac{f_i}{f_{rc}}}}_{C_2(f_i)} \underbrace{\frac{z}{z - e^{j2\pi f_i T_s}}}_{\text{input sinusoid}} e^{j2\pi f_i t_0} \tag{B.45}$$

$$E_n(z) = C_2(f_i) \frac{z}{(z - e^{-2\pi f_{rc} 2p_0 T_s})(z - e^{j2\pi f_i T_s})} e^{j2\pi f_i t_0} \tag{B.46}$$

Doing partial fraction expansion:

$$E_n(z) = C_2(f_i) \left[\underbrace{\frac{1}{e^{j2\pi f_i T_s} - e^{-2\pi f_{rc} 2p_0 T_s}} \frac{z}{z - e^{j2\pi f_i T_s}}}_{\text{steady state}} + \underbrace{\frac{1}{e^{-2\pi f_{rc} 2p_0 T_s} - e^{j2\pi f_i T_s}} \frac{1}{z - e^{-2\pi f_{rc} 2p_0 T_s}}}_{\text{initial value}} \right] e^{j2\pi f_i t_0} \tag{B.47}$$

When we are applying this in the frequency domain, the initial value response is not important. When doing a frequency domain approach we assume that the sinusoids making up the input signal have been on the input of the circuit for all time. We are not interested in startup phenomenon. Therefore, the value of E_n in the time domain at the t_0 time instants is given by:

$$E_n = V_{out}(nT_s + t_0) = \frac{(e^{j2\pi f_i p_0 T_s} - e^{-2\pi f_{rc} p_0 T_s})(-e^{j2\pi f_i \frac{1}{2} T_s} + e^{-2\pi f_{rc} p_0 T_s})}{e^{j2\pi f_i T_s} - e^{-2\pi f_{rc} 2p_0 T_s}} \frac{1}{1 + j\frac{f_i}{f_{rc}}} e^{j2\pi f_i (nT_s + t_0)} \tag{B.48}$$

$$E_n = V_{out}(nT_s + t_0) = -\frac{e^{j2\pi f_i p_0 T_s} - e^{-2\pi f_{rc} p_0 T_s}}{e^{j2\pi f_i \frac{1}{2} T_s} - e^{-2\pi f_{rc} p_0 T_s}} \frac{1}{1 + j\frac{f_i}{f_{rc}}} e^{j2\pi f_i (nT_s + t_0)} \tag{B.49}$$

Since the input is defined as $V_{in}(t) = e^{j2\pi f_i t}$, we can define a sort of transfer function relating the value of V_{out} at the instant t_0 to the input sinusoid. This transfer function is defined as G_0 in the following way:

$$V_{out}(nT_s + t_0) = G_0(f_i) e^{j2\pi f_i n T_s} \tag{B.50}$$

$$G(f_i) = -\frac{e^{j2\pi f_i p_0 T_s} - e^{-2\pi f_{rc} p_0 T_s}}{e^{j2\pi f_i \frac{1}{2} T_s} + e^{-2\pi f_{rc} p_0 T_s}} \frac{1}{1 + j\frac{f_i}{f_{rc}}} \tag{B.51}$$

$$G_0(f_i) = G(f_i) e^{j2\pi f_i t_0} \tag{B.52}$$

The difference equation for phase 2 (equation B.38) can be formed from the difference equation for phase 0 (equation B.39) by substituting $e^{j2\pi f_i t_0} = -e^{j2\pi f_i t_2}$. The same substitution in equation B.52 results in the expression for $G_2(f_i)$:

$$V_{out}(nT_s + t_2) = G_2(f_i)e^{j2\pi f_i nT_s} \tag{B.53}$$
$$= -G(f_i)e^{j\omega_i t_2}e^{j2\pi f_i nT_s} \tag{B.54}$$

Now equations B.37 and B.39 give the expressions for G_1, G_3 and G_4:

$$V_{out}(nT_s + t_1) = G_1(f_i)e^{j2\pi f_i nT_s} \tag{B.55}$$
$$= -G(f_i)e^{j2\pi f_i t_2}e^{j2\pi f_i nT_s} \tag{B.56}$$
$$V_{out}(nT_s + t_3) = G_3(2\pi f_i)e^{j2\pi f_i nT_s} \tag{B.57}$$
$$= G(f_i)e^{j2\pi f_i t_4}e^{j2\pi f_i nT_s} \tag{B.58}$$
$$V_{out}((n+1)T_s + t_0) = G_4(f_i)e^{j2\pi f_i nT_s} \tag{B.59}$$
$$= G(f_i)e^{j2\pi f_i t_4}e^{j2\pi f_i nT_s} \tag{B.60}$$

In summary:

$$V_{out}(nT_s + t_k) = G_k(\omega_i)e^{j\omega_i nT_s} \tag{B.61}$$

$$G(f_i) = -\frac{e^{j2\pi p_0 \frac{f_i}{f_s}} - e^{-2\pi p_0 \frac{f_{rc}}{f_s}}}{e^{j2\pi \frac{1}{2}\frac{f_i}{f_s}} + e^{-2\pi p_0 \frac{f_{rc}}{f_s}}} \frac{1}{1 + j\frac{f_i}{f_{rc}}} \tag{B.62}$$
$$G_0(f_i) = G(f_i)e^{j2\pi f_i t_0} \tag{B.63}$$
$$G_1(f_i) = -G(f_i)e^{j2\pi f_i t_2} \tag{B.64}$$
$$G_2(f_i) = -G(f_i)e^{j2\pi f_i t_2} \tag{B.65}$$
$$G_3(f_i) = G(f_i)e^{j2\pi f_i t_4} \tag{B.66}$$
$$G_4(f_i) = G(f_i)e^{j2\pi f_i t_4} \tag{B.67}$$

Figure B.2: Tayloe Mixer Double Balanced G_k

Bibliography

[1] D. Tayloe: *Ultra low noise, high performance, zero IF quadrature product detector and preamplifier*, March 2003

[2] D.H. van Graas: *The fourth method: Generating and Detecting SSB Signals*, QEX, September 1990

[3] Yasuo Nozawa: *The Merigo Method:SSB Generator/Producing A Demodulator*, HAM Journal Magazine, July/August 1993

[4] H. Pekau, J.W. Haslett: *A 2.4GHz CMOS Sub-Sampling Mixer With Integrated Filtering*, IEEE journal of solid state circuits, vol.40 no.11, November 2005

[5] D. Jakonis, C. Svensson: *A 1.6 GHz Downconversion Sampling Mixer in CMOS*, ISCAS 2003, vol. 1, May 2003

[6] T. Strom, S. Signell: *Analysis of periodically switched linear networks*, IEEE transactions on circuits and systems, vol cas-24, no 10, October 1977

[7] B. Leung: *VLSI for Wireless Communication*, Prentice hall electronics and VLSI series, New York: 2002 ch. 4

[8] B. Nauta, E. Seevinck:*Linear CMOS Transconductance Element for VHF Filters*, Electronic Letter, vol.25 no. 7, March 1989

[9] E.A.M. Klumperink, B. Nauta: *Systematic Comparison of HF CMOS Transconductors*, IEE transactions on circuits and systems-II: analog and digital signal processing, vol. 50 no. 10, October 2003

[10] B. Razavi: *Design Considerations for Direct-Conversion Receivers*, IEE transactions on circuits and systems-II: analog and digital signal processing, vol. 44 no. 6, June 1997